University College of Southeast Norway

Photon Absorption Enhancement of TiO_2 Nanotube Arrays Decorated with Aluminum Nanoparticles

Shuai Zhang

Master of Micro and Nano Systems Technology

Submission date: May 2017
Supervisor: Kaiying Wang

University College of Southeast Norway
Department of Micro Systems

Photon Absorption Enhancement of TiO_2 Nanotube Arrays Decorated with Aluminum Nanoparticles

Shuai Zhang

IMS, HSN

shuai.zhang@student.hbv.no

Abstract

In this thesis, well-aligned TiO_2 nanotubes (TNTs) decorated with aluminum nanoparticles have been fabricated by electrochemical anodization and subsequently magnetron sputtering technique. UV-vis spectroscopy analysis indicate that photon absorption spectrum of crystallized TNTs with Aluminum nanoparticles is extended to visible light band with strong absorption (wavelength 400 – 800 nm). Photocurrent characteristics of the TNTs/Al show that the plasmonic nanoparticles Al contribute extra electron-hole pairs to enhance photocurrent under visible light illumination, which further indicate electrons generation, separation and transportation in this system. This thesis gives a systematic study of the subject for photon absorption enhancement of TiO_2 nanotube arrays decorated with aluminum nanoparticles.

Acknowledgements

I would like to thank Professor Kaiying Wang for the opportunity of pursuing master studies under his supervision. Thank you for highly motivation and all the lively discussions always remained very inspirational. Thanks for the instructions of my thesis, which teach me is not only scientific knowledge but also teamwork.

Special thanks to Mr. Kang Du for improving the scientific writing of my thesis and for helping me with experiment and all the problems I met during my measurements. I am grateful for your enthusiasm and patience every time.

A special thanks to Xiao Fan, for help with suggestions in the project.

I would like to express my appreciation to Zekija Ramic for the helping experimental preparation and measurements in both clean room and bio-lab for more than one year.

Acronyms

TNTs	TiO_2 nanotubes
TNTAs	TiO_2 nanotubes arrays
SEM	Scanning electron microscopy
XRD	X-ray diffraction
XPS	X-ray photo-electron spectroscopy
CV	Cyclic voltammetry
EIS	Electrochemical impedance spectroscopy
NPS	Nanoparticles
LSPR	Localized surface plasmon resonance

List of Figures

Contents

Chapter 1 Introduction

1.1. Background

It is generally agreed that the planet of earth and all organics on the earth rely on solar energy. As the basic electromagnetic radiation, light carries energy, which connects to the process of physics, chemistry, biology and so on. Due to the fact that fossil fuels are over-consumed, there is a natural trend to explore alternative approaches to serve human activities through light harvesting and its conversion into usable forms. Nowadays existing methods mainly exercise through the platform of photoelectric, photothermal, photo-thermal-electric conversions etc. Especially, photocatalysis provides a scheme that can accomplish chemical transformations utilizing solar energy and therefore store chemical energy[1]. As an excellent material electrode, TiO_2 is receiving remarkable attention and are extensively studied in the area of photocatalysis applications. TiO_2 nanotubes have higher photocatalyst and can improve the photoelectron transfer efficiency; they are also cheap and non-toxic[2]. However, the bandgap of TiO_2 (anatase 3.2 eV and rutile 3.0 eV) limits their light absorption to UV irradiation (<387 nm, accounting for 4∼5% of solar spectrum) as well as efficiency of photo energy conversion. Therefore, various strategies have been utilized to modify properties of TiO_2 nanomaterials, including gas phase process, metal and nonmetal decoration, dyes sensitization, and coupling with narrow band-gap semiconductors. Among these approaches, TiO_2 nanotube arrays decorated with metal nanoparticles shows much advantages for achieving high performance, such as plasmon-enhanced solar desalination, plasmon-photocurrent enhancement, plasmon-enhanced catalytic reactions[3].

As an advanced technique, plasmonic photocatalysis greatly contributes to TiO_2 photocatalytic ability in quickly decomposing organic compounds. Such technique utilizes localized surface plasmon resonance (LSPR) to form reformative local electromagnetic fields around the TiO_2 photocatalyst to enhance the photocatalytic

optical trapping capability and photoelectric conversion rate. The key is to fabricate precisely controlled nanostructures so that the LSPR spectrum is sufficiently coupled with the incident light. In this case, plasmonics enhances light absorption and extends TiO_2 absorption to a broad band.

In terms of the academic preference of plasmonics, metal-based ones have generated the most hot debates in the field of solar energy conversion, stemming from the fact that they have powerful visible plasmonic responses of overlapping with the solar spectrum[4]. The excitation of localized surface plasmons (LSP) on the surface of metallic nanostructures produces intense electric field amplitudes that can increase light absorption, thereby, improving the electrochemical activities of TiO_2[5]. Nevertheless, based on the fact that plasma frequency of aluminium is priority to that of gold or silver, thus results to visible dramatic plasmonic response. Previous mainstream studies of aluminium plasmonics concentrates on biological sensors or photocatalysis, which requires strong absorption. Consequently, tuning the plasmonic resonances of aluminium for a wide range of wavelengths, especially towards the visible regime, becomes quite favorable but challenging[6].

In this thesis, we focus on loading aluminum nanoparticles product on TNTs by a facile decoration technique, expecting to enhance visible light absorption as well as their photocurrent. Amount of the aluminum nanoparticles on crystalline anatase nanotubes were tuned by magnetron sputtering deposition technique with different thickness of aluminum nanoparticles. Microstructure and photon spectrum absorption properties of the decorated nanotube composites examined by physical techniques such as scanning electron microscopy (SEM) and UV-Visible absorption spectroscopy are reported. Meanwhile, I-V characteristics and transient photocurrent responses of the decorated TNTs composites are characterized by photoelectric measurement method, further revealing intrinsic characteristics of electron generation, separation, and transportation in TiO_2-Al systems.

1.1.1 The introduction of plasmonic effect

In terms of both infrared and optical frequencies, plasmonics is supposed to have great advantage of transformative applications in optics-based technologies. In the past few years, applications and related devices in the fields of plasmon-enhanced light harvesting, photocatalysis, surface-enhanced spectroscopies, optics-based sensing, nonlinear optics, and active optoelectronic have enormous improvement.

1.1.1.1. Plasmon

With respect to physical point of view, plasmon is a quantum of plasma oscillation. Being similar to the argument that light, or optical oscillation, is made up of photons, plasma oscillation is made up of plasmons. Plasmon could be treated as quasiparticle due to the fact that it is generated from quantization of plasma oscillations, in the same as phonons are quantizations of mechanical vibrations. Therefore, plasmons are not only collective but also in a discrete number of oscillations of the free electron gas density. For instance, at the horizon of optical frequencies, plasmon polartion is created from the combination of plasmons and photon[7].

1.1.1.2. Surface plasmon resonance

SPR, surface plasmon resonance is the resonant oscillation of conduction electrons, especially via permittivity material stimulated by incident light, either positively or negatively. As soon as the frequency of incident photons and the natural frequency of surface electrons are matched with each other, resonance condition is then established. SPR in subwavelength scale nanostructures can be polaritonic or plasmonic in nature.

Aiming to measure the material adsorption onto typical planar metal of gold or silver surfaces or onto metal nanoparticles[8], SPR is applied as the basic standard tool, which is suggested as the foundational principle behind applications of color-based biosensor and various lab-on-a chip sensors[9].

Propagating in the same direction to the negative permittivity material surface, the surface plasmon polariton is treated as a typical non-radiative electromagnetic surface wave. Due to the fact that such wave is on the boundary of the conductor and external medium like air, water and vacuum, oscillations shows high sensitivity to any change of the boundary, for instance, molecules adsorption to conducting surfaces [10].

Different models based on quantum theory, Drude model, are able to demonstrate the existence and properties of surface plasmon polaritons. Take the most straightforward way to handle this problem, each material is proposed to be treated as a homogeneous continuum, described by a frequency-dependent relative permittivity between the external medium and the surface[11]. Therefore, named as the materials' "dielectric function", the quantity is complex permittivity. Aiming to meet the terms of describing the electronic surface plasmon to exist, the real part of the dielectric constant of the conductor must be negative and its magnitude must be greater than that of the dielectric. Such condition can be satisfied for interfaces of air/metal or water/metal, especially in the region of infrared-visible wavelength, where the real dielectric constant of a metal is negative and that of air or water is positive[12].

Excited by light, localized SPRs, or LSPRs, are collective electron charge oscillations in metallic nanoparticles. LSPRs exhibit enhanced near-field amplitude at the resonance wavelength. Such field has been greatly localized in the horizon of nanoparticle, and has been quickly decayed away from the nanoparticle/dieletric interface into the dielectric background, even though far-field scattering by the particle is also improved by the resonance. As an essential aspect of LSPRs, light intensity enhancement plays an important role, and localization stands for the truth that LSPR own high spatial resolution or subwavelength, additionally limited only by the size of nanoparticles. Due to the improvement of field amplitude, effects depending on the amplitude are enhanced by LSPRs as well[13]. A typical example sees the magneto-optical effect.

1.1.1.3. Plasmonic nanoparticles

The concept of plasmonic nanoparticles is defined as particles whose electron density is able to match electromagnetic radiation of wavelengths that are fairly greater than the particle resulting from the instinct of dielectric-metal interface between the medium and the particles. In detail, different from a pure metal who has a maximum limit on size wavelength, requiring the size wavelength to be effectively combined based on the material size.

Plasmonic nanoparticles show amazing scattering, absorbance, and coupling properties due to their geometries and relative positions, thus particles are different from ordinary surface plasmons[14]. A hot-debated research has been generated in the applications of solar cells, spectroscopy, signal enhancement for imaging, and cancer treatment due to these particular properties.

Clusters and related plasmonic molecules are formed by nanoparticles, afterwards, nanoparticles affect each other to form cluster states. The nanoparticle symmetry and corresponding distribution of electrons influence a kind of bonding or anti-bonding feature between nanoparticle and molecular orbitals[15]. Polarized light are utilized to manage the electrons distribution because that light couples with the electrons. Adjusting the nanoparticles' geometry is applied to manipulate the optical activity and properties of the system, however, furthermore, polarized light can also meet this requirement by lowering the symmetry of the conductive electrons inside the particles and changing the dipole moment of the cluster. To manipulate light on the nano scale, the above mentioned clusters are quite helpful.

1.1.2. Aluminum nanoparticles for plasmonics

Many papers have discussed plasmon performance topics related to gold, silver, and other materials. However, the above mentioned noble metals have drawbacks hindering the development of plasmonic devices towards the blue and ultraviolet (UV) parts of the EM spectrum. Firstly, gold does not exhibit plasmonic resonances at wavelengths

shorter than 520 nm due to its interband transitions[16]. Secondly, silver nanostructures exhibit LSPRs down to 350 nm but suffer from strong oxidation and lose plasmonic properties over time. In order to cope with these limitations, aluminium plasmonics appears. Aluminum does good in supporting surface plasmons in the visible and UV, due to its intrinsic properties, such as its high plasma energy of 15.6 eV, aluminium behaves like a metal up to energies located in the deep UV, while keeping relatively low losses, except within a relatively narrow energy range centred at 1.5 eV where interband transitions are active[17]. Opposite to noble metals, aluminium is inexpensive and easily-access as it is widely distributed on Earth. Such feature becomes an enormous advantage in industrial applications which potentially shows profound impact on economic benefits. Therefore, having the energy to create a new optoelectronic market, aluminium contributes to plasmonic engineering of optical properties of wide bandgap semiconductors[18]. However, common plasmonic materials like silver and gold both have plasmonic bands in the visible range and extension of the LSPR response into the UV region is difficult due to the intrinsic limitations of the noble metals. Different from silver and gold, aluminum presents material properties that allow strong plasmon resonances spanning much of visible region of the spectrum and into the ultraviolet.

Aluminum is an alternative plasmonic material with an extended response into the visible region. The extended response in conjunction with the low cost and convenient manufacturing makes aluminum promising in UV plasmonics applications, such as surface-enhanced fluorescence, surface-enhanced Raman scattering, and photovoltaics[19].

1.1.3. The influence factors of aluminum nanoparticles for plasmonics

The plasmonic response of aluminum nanostructures is supposed to depend sensitively on the presence of the factors of aluminum nanoparticles, such as the diameter of Aluminum nanoparticles, the thickness of the aluminum nanoparticles.

1.1.3.1. The diameter of Aluminum nanoparticles

In figure.1.1, the extinction spectra of Al nanoparticles in different diameters are presented. As the particle size increases, the Al spectrum exhibits significant redshift and broadening on account of retardation effects and emergence of higher order plasmon modes. When the diameter of nanoparticle raises, the LSPR is red-shifted and becomes broader. Such change results from phase delay across the nanoparticles decreasing the plasmonic resonance lifetimes. Because of phase delay, field spectra presents extra peaks with lower wavelengths and lower relative intensities. These peaks correspond to the signature of high order plasmonic resonances sustained by larger Al diameter as well[20].

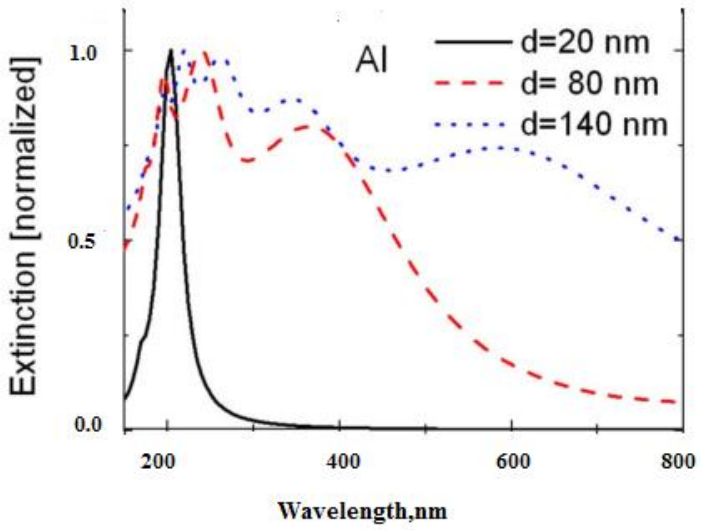

Figure 1.1. Calculated extinction spectra of spherical Al nanoparticles with diameters of 20, 80, and 140 nm [21]

1.1.3.2. Plasmon energy depends on the Al_2O_3/Al fraction

Figure 1.2 shows the scattering efficiency spectra of 100 nm diameter aluminum nanoparticles with varying metal oxide[22]. Aiming to calculate the effective di-electric function for each composite metal film, Al fractions are obtained by fitting the ellipsometrically measured Drude dielectric functions with the Bruggeman dielectric function, yielding n_{Al} = 0.91 (green), 0.81 (blue), and 0.73 (orange).

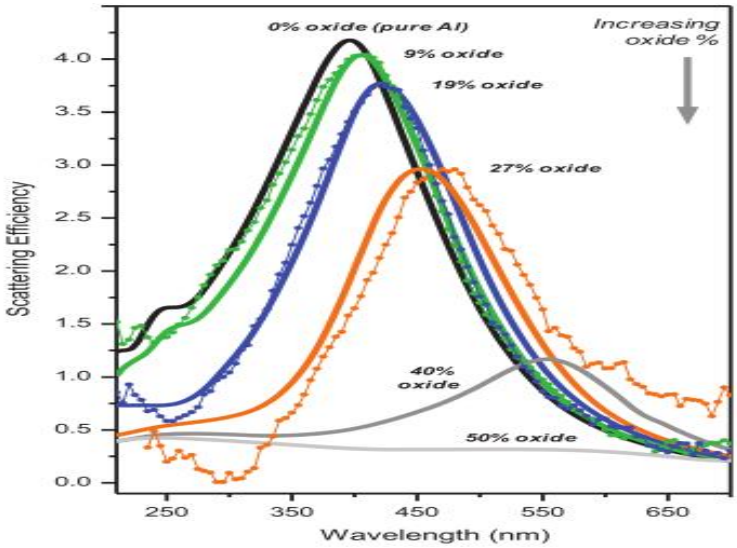

Figure 1.2. Scattering spectra of 100 nm diameter nanodisks with varying metal oxide fractions[23].

The Bruggeman model allows the calculation of a composite Al/Al_2O_3 dielectric function ε by combining the tabulated values of pure Al and Al_2O_3 as [(1.1),(1.2)]

$$nAl\left(\frac{\varepsilon_{Al}-\varepsilon}{\varepsilon_{Al-2\varepsilon}}\right)+\left(\frac{\varepsilon_{Al}-\varepsilon}{\varepsilon_{Al+2\varepsilon}}\right)=0 \quad (1.1)$$

where n_{Al} and n_{ox} are the volume fractions of aluminum and oxide comprising the material, severally. The Al dielectric function for each film was derived from the ellipsometric data assuming a bilayer composed of a thin dielectric Al_2O_3 layer ($\varepsilon_{ox} = \varepsilon_{Al2O3}$) coating an infinitely thick metallic Al substrate characterized by a modified Drude response

$$\varepsilon_{ox} = \varepsilon_{\infty} - \frac{w_p^2}{w^2+iw\Gamma} \quad (1.2)$$

in which ω_p is the bulk plasmon frequency, Γ is the damping constant, and ε_∞ is the high-frequency response. To capture experimental errors, all films exhibited similar

surface oxide thicknesses (2-6 nm) and metallic Drude damping ($\boldsymbol{\Gamma} \approx 0.9$-$1.3$ eV) and ε_∞ (3-4) parameters[24].

Al nanoparticles in Figure 1.2 demonstrates that the plasmon energy depends sensitively on the fraction of Al_2O_3 in core metal. As Al_2O_3 fraction increases, the scattering efficiency decreases. That is to say, for Al nanostructures of the same geometry with the same native oxide shell, the core Al_2O_3/Al fraction is a fundamental element of the optical response[25]. These findings imply that the need of reproducible Al-based UV plasmonic nanostructures is fabrication in a pristine environment to minimize the deleterious effects of the bulk metal oxide. An assessment of the oxide fraction could be obtained by matching the spectrum of a foregone plasmonic nanostructure with spectra calculated using the Bruggeman effective medium approximation[26]. The above arguments set the cornerstone to develop Al nanostructures for novel UV and visible range plasmonic applications, ultimately enabling high-area, low-cost, CMOS-compatible plasmonic devices and applications not currently possible with noble and coinage metals.

1.1.4. Fabrication of methods of aluminum nanoparticles

Traditionally, researchers have applied the physical vapor deposition (PVD) method to deposit aluminum nanoparticles. Techniques for the deposition of aluminum nanoparticles on substrates have emerged very recently. These can be classified into two types: physical and chemical methods. Physical techniques include evaporation deposition, sputtering deposition, chemical methods are able to ensure intimate contact of the nanoparticles with the substrates[27].

1.1.4.1. Evaporation method

The setup for thermal evaporation is shown in Figure 1.3. Taking aluminum as an example of a source, aluminum vapor is generated if the temperature is higher than its evaporation point. The vacuum enables vapor particles to travel to the target object of

substrate directly, with increasing the temperature further, the growth of aluminum film occurs, which leads to intimate contact of the film with the substrate. The most vital precondition for thermal evaporation machine to occur is that the metallic source must be easily vaporized[28]. Normally, aluminum is evaporated in a vacuum at high temperature. Our group has successfully deposited uniform and dense aluminum nanoparticles on various substrates, such as FTO glass, quartz glass, and glass. Numerous nanoparticles can be observed on the surface, the size, shape, thickness, and structure of the aluminum nanoparticles can easily be controlled by the temperature and the relevant current. Briefly, thermal evaporation machine can deliver highly uniform aluminum nanoparticle films on various substrates and can be used as a facile method to tune the morphology and thickness of the films.

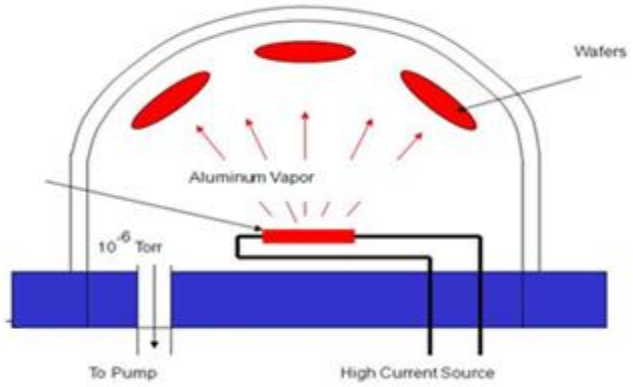

Figure 1.3. Thermal evaporation method for aluminum deposition[29]

Nevertheless, a large amount of laboratories still work on evaporation, such technique has been gradually replaced by sputtering in most micro technologies due to certain reasons. In terms of covering step problem, the thickness of metal layers is constantly raised by the lateral dimensions of transistors. Thermal evaporated films do bad in covering these structures which yield a discontinued film on the vertical walls. In addition to this, producing well-controlled alloys by evaporation method remains difficult[30].

1.1.4.2. Sputtering

Following Figure 1.4, Physical Vapor Deposition (PVD) by sputtering method is quite helpful to deposit nanoparticles aluminum. With respect to sputtering method, vacuum chamber places both target material and the substrate, and a voltage is applied between them. Consequently, the target acts as the cathode, whereas the substrate acts as the attachment of the anode. Ionizing a sputtering gas, for example chemically inert or heavy gas like Argon, generally creates a plasma. The sputtering gas bombards the target and sputters off the material we are attempting to deposit[31]. As the gas pressure raises, the ions collide with the gas atoms that act as a moderator and move diffusively, reaching the substrates or vacuum chamber wall and condensing after undergoing a random walk. The whole range from high-energy ballistic influence to low-energy thermalized motion is available by adjusting gas pressure. Unlike thermal evaporation, sputtering is widely applied in semiconductor industry to deposit thin films of different materials in the process of integrated circuit. Regarding to optical application, sputtering also deposits anti-reflection coatings on glass. Due to low substrate temperatures, sputtering remains ideal to deposit metals for thin-film transistors. Thus, materials with very high melting points are easily sputtered while evaporation of these materials in a resistance evaporator is difficult and problematic, which is considered as the most distinctive superiority of sputtering method[32].

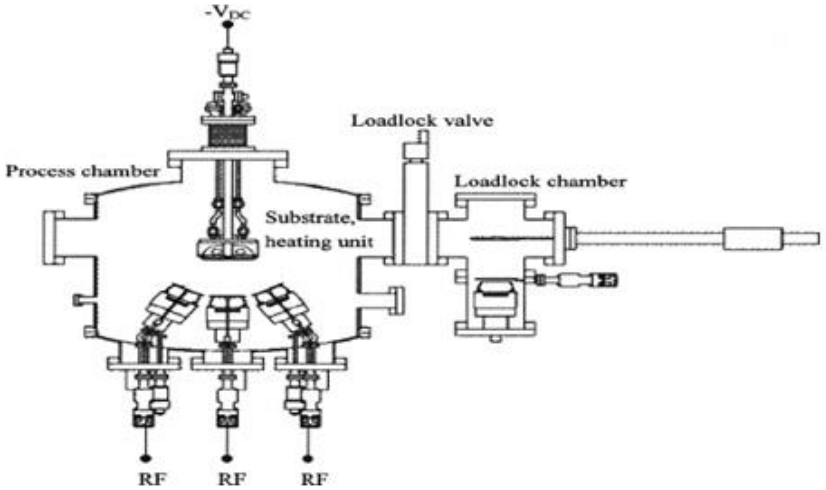

Figure 1.4. Sputtering method for aluminum deposition[33]

1.1.4.3. Chemical method

(1) Al nanoparticle synthesis methods via chemical reduction

Paskevicius et al. developed a mechanochemical synthesis method typically for pure Al nanoparticles. Such technique utilized aluminium chloride ($AlCl_3$) as the precursor and either sodium (Na) or lithium (Li) metals as the reducing agents. At room temperature inside a ball mill, the solid-state reaction worked. X-ray scattering measurements gave out an average value of 55nm for the synthesized Al nanoparticles. Equation of (1.3) and (1.4) reveal the reduction process with Li and Na correspondingly[34].

$$AlCl_3+3L \rightarrow Al+3LiCl \quad (1.3)$$

$$AlCl_3+3N \rightarrow Al + 3NaCl \quad (1.4)$$

Chung et al. applied a N,N-dimethylethylamine alane solution (AlH_3) which had catalytic amounts of titanium isopropoxide ($Ti(O\text{-}Pr)_4$) added to form Al nanoparticles via reduction and decomposition means of the alane solution, the synthesized Al nanoparticles were 20–30nm in size. The Equations is shown in Equation (1.5).

$$AlH_3+Ti(O\text{-}Pr) \rightarrow Al \rightarrow Al_n \quad (1.5)$$

Parallel studies using alane decomposition and reduction to synthesize Al nanoparticles see Jouet et al. Their group selected organic molecules following that of perfluorinated carboxylic acids as passivation and stabilizing agents in an alane reduction reaction to control the size of the Al nanoparticles[35]. Purdy et al. used a mixture of aluminium halide alkoxide in a solution of toluene, which was treated with the reducing agent of sodium potassium alloy to synthesize Al nanoparticles. On the basic of the past researches, it is referred that in some special cases, Li powder also played the role of the reducing agent[36]. For example, Haber and Buhro used two direct chemical reduction methods to synthesize aluminum nanoparticles. The Al nanoparticle sizes varied between 45 and 180 nm. In both methods, it is obvious that effects of 1,3,5-trimethylbenzene solution work as a medium for the reducing reaction to take place. Equation (1.6) and (1.7) demonstrate the detail of the both methods[37].

Method A

$$3LiAlH_4 + AlCl_3 \rightarrow (1,3,5\text{-}Me_3C_6H_4 \text{ at } 164\ ^\circ C) \rightarrow 4\text{nano-Al} + 3LiCl + 6H_2 \quad (1.6)$$

The reaction of lithium aluminum hydride, $LiAlH_4$ with aluminum chloride ($AlCl_3$) in a solution of 1,3,5-trimethylbenzene produced Al nanoparticles with an average mean coherence length of 160±50 nm. In this reaction, $LiAlH_4$ served as the reducing agent.

Method B

$$H_3Al(NMe_2Et) \rightarrow (1,3,5\text{-}Me_3C_6H_3 \text{ at } 164\ ^\circ C, \text{ with or without } Ti(O\text{-}i\text{-}Pr)_4) \rightarrow \text{nano-Al} + (3/2)H_2 + NMe_2Et \quad (1.7)$$

In method B, Al nanoparticles were prepared via the reduction of dimethylethylamine alane, H3Al(NMe_2Et) in a solution of 1,3,5 trimethylbenzene. Refluxing between 100 and 164 ℃ can be treated as a combination solution. The addition of the decomposition catalyst $Ti(O\text{-}i\text{-}Pr)_4$ was a matter of choice. If $Ti(O\text{-}i\text{-}Pr)_4$ was not added, the reduction process would happen at a higher temperature of 164 ℃. The synthesized mean particle sizes were between 40 and 180 nm.

Compared to method A and other potential synthesis methods, method B has great advantage of tight and safe setup in providing Al nanoparticles with a lower oxide content and coarser oxide distribution. To control the synthesized particle sizes and to provide a wide range of particle size, chemical reduction synthesis method plays a useful role. In addition, such method offers a straightforward way to up-scale, which satisfies various nanoparticles-manufacturing requirement.

1.1.5. Other fabrication of methods of metal nanostructures

As an efficient tool for plasmonic nanostructures' fabrication, electron beam lithography (EBL) is demonstrated in Figure 1.5[38]. Firstly, a scanning electron beam exposes a positive resist before spinning coated on a substrate, which enables the favorable pattern shape to be written down in the resist. The electrons and the resist are correlated with each other, which contributes to break the polymeric chains. Compared to the non-exposed area, as the exposed areas becomes smaller chains with high

solubility, a selective solvent style resist is established. At this time, the whole sample is set up in metallic evaporation techniques. To make the metal evaporated, it is of vital importance to have an inverted profile. Actually, the discontinuity between the substrate metal and the resist is mandatory in the last step of resist removal. Furthermore, to prevent contact, a minimum ratio of 1:3 for the metal resist thickness is applied. Finally, the sample is dipped in a solvent dissolving the remaining resist and lifting up the unwanted metallic areas. In detail, aluminium can be evaporated by using either electron-beam or thermal evaporation, with a typical deposition rate between 0.1 nm s^{-1} and 0.2 nm s^{-1} and a base pressure between 10^{-6} and 10^{-7}Torr. All above mentioned experimental conditions focus on keeping a relatively smooth surface. Whereas it is hard in the aluminium evaporation due to its tendency to nucleate in the early stage of growth. This adds difficulty to achieve a smooth Al nanostructure surface, which exhibits large grain size leading to distorted shapes. These features are to some extent visible on the scanning electron microscopy, shorting for SEM, images of lithographed aluminium nanostructures presented in this thesis.

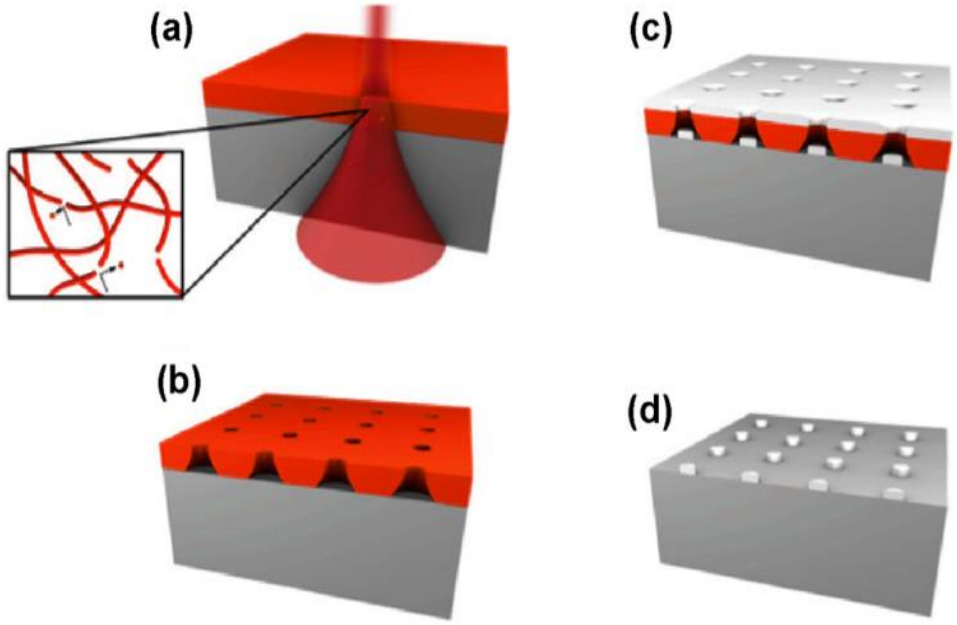

Figure 1.5. Main steps of EBL for the deposition of aluminum nanostructures. (a) Electron beam (pink colour) exposure of the resist (red colour) leading to polymeric chain breaking (inset). (b) Inverted resist profile after development. The profile shape stems from overexposure at the resist substrate interface. (c) Metal coating (grey colour) and (d) the remaining metallic nanostructures after the stripping of the resist in a solvent[38].

Figure 1.6 presents Colloidal lithography (CL) [39]. A generally-accepted version of NSL is the application of organized 2D colloidal crystals with a hexagonal close-packed pattern as an evaporation mask, usually in combination with reactive ion etching. The subsequent evaporation through the mask defines the resulting metallic pattern, and the material deposition conditions, for example the evaporation angle or specific deposition technique (electron beam deposition, sputtering, epitaxial growth, thermal deposition),zhe enable the variation of the final pattern. The most controversial step of CL is establishing a well-organized 2D colloidal layer with as few defects as possible (such as dislocations in the colloidal crystal, or vacancies). Arranging the colloids contained in commercial solutions onto the substrate helps to obtain colloidal crystal formation. Several methods are commonly utilized to meet the goal, including drop-coating, spin-coating, dip-coating, electrophoretic deposition, or self-assembly at the gas–liquid interface etc. A surfactant can be added to the solution to assist the colloids in wetting the substrate, or functionalized colloids are purchasable to avoid aggregates and to form a homogeneous thin layer. It is reasonable to take NSL leading to aluminium nanotriangles for reference. Here the hexagonal 2D pattern of polystyrene beads are applied as the evaporation mask leading to the nanotriangles of aluminium. Combining scanning electron microscope and atomic force microscopy characterize native alumina shell in this paper. So the existence of the alumina layer, especially on the tips of the nanotriangles, leads to a dramatic red shift of the LSPR maximum or λmax. By combining the samples to different solvents, it is also experimentally exhibited that the plasmonic resonances sustained by aluminium nanotriangles.

Alternatively, Figure 1.7 measures the fabrication of metallic nanostructures on dielectric by the method of Interference lithography (LIL or IL) [41]. Allowing for periodic nanostructures, IL still has great merits due to its maskless process, economic efficiency, time-saving and large-scale compatible. In detail, let us emphasize on the principle of IL. A layer of photoresist prints the interference patterns, either between two or among more coherent light waves. As the exposing step passing by, the selected solvent dissolves the illuminated areas, and the patterns are printed in the photoresist.

However, the potential drawback of IL stems from the resolution of the photosensitive resist, which is identified by the half of the wavelength of the laser source, standing for the fact that short wavelengths are required to obtain the nanostructures. As a result, as the combination of IL with extreme ultraviolet light from undulators at synchrotron radiation facilities, extreme ultraviolet IL (EUV IL) has become a hot-debated issue. Using EUV IL, aluminium nanoparticles arrays with size down to 40 nm and well-defined geometries has been deposited over large areas. In this paper, EUV IL has been employed to create arrays of nanoholes in the resist, and the subsequent evaporation led to the aluminium nanoparticle arrays. These nanoparticles exhibit strong and sharp plasmonic resonances in the near and mid-UV spectral regions as confirmed by experiments and theory.

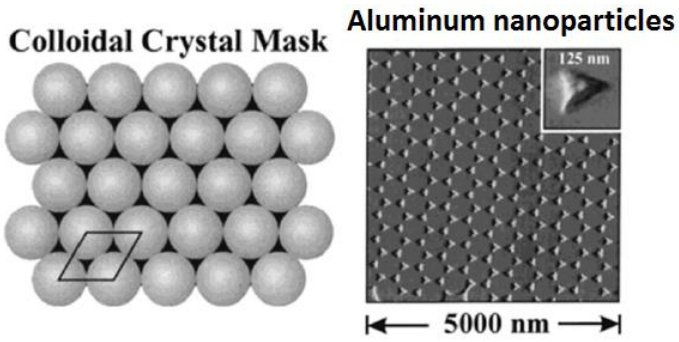

Figure 1.6. Schematic illustration of hexagonal compact arrays of microbeads used as an evaporation mask (left panel) and subsequent arrays of aluminum nanotriangles after the evaporation and the bead's removal (right panel) [40]

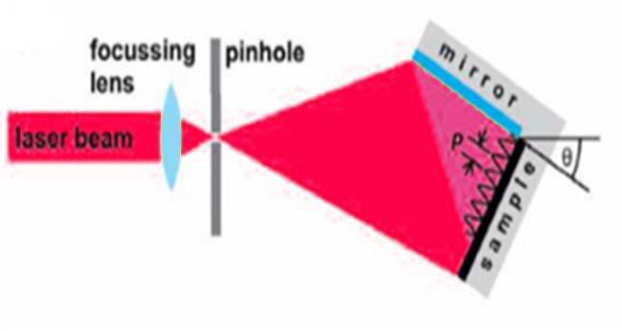

Figure 1.7. Schematic of the laser interference lithography setup[41]

Pressing through a structured map like Figure 1.8, Nanoimprint Lithography (NIL) relies on the mechanical deformation (and its subsequent patterning) of the resist material[42]. Based on the fact that NIL technique is able to produce nanostructures in big ares on the substrate in short time, it is popular in industrial applications. In reality, compared to other lithography methods, using nanoimprinting is the production of stamps, it is reusable many times and well suited for integrating into large-scale rollers in a roll-to-roll process. The utility of NIL fabrication of aluminium nanostructures has already generated attraction in the area of plasmonic application. For UV-SERS detection aim, large scale Al nanovoid substrates have been fabricated. Related methods integrate ion milling, nanoimprinting and e-beam evaporation, measuring up tp 180nm in diameter and 20 nm in depth. And over 1cm^2 substrate is easily covered in a nanovoid array. This paper reveals that the UV Raman signal with a 244nm laser excitation of adenine by more than three orders of magnitude compared to planar metal substrates has been enhanced both inside or at the edge of the nanovoids. These UV-SERS plasmonic substrates produce great attraction in the operating field of sensitive sensing or biochemical.

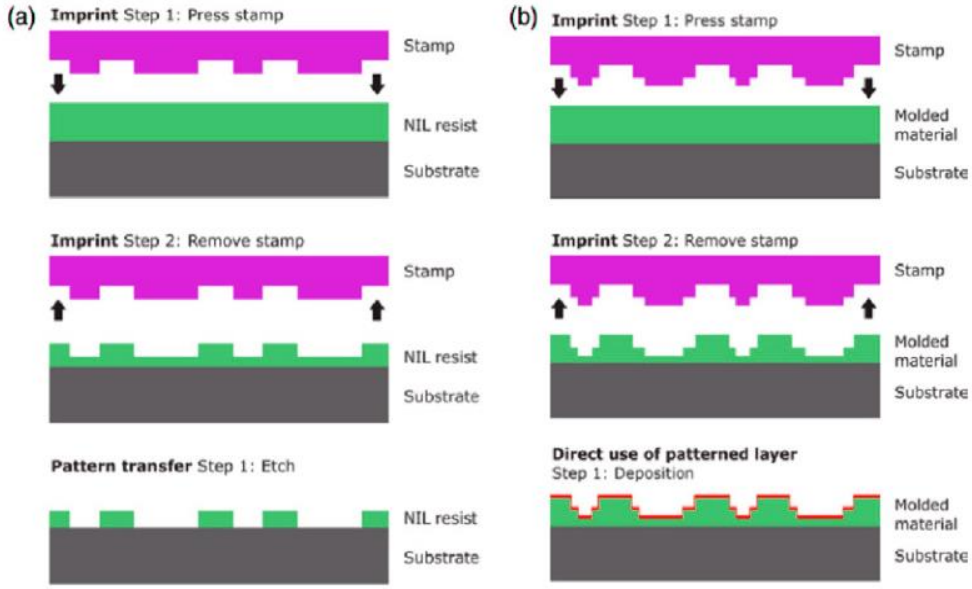

Figure 1.8. Schematics of nanoimprint processes: (a) the originally proposed nanoimprint lithography process where a resist layer is used for further pattern transfer, as in standard lithography, and (b) a method where the patterned layer is directly used (shown here with the deposition process as the last fabrication step) [44].

Table 1 the fabrication methods of Aluminum plasmonic nanostructures, resonance range and their applications

Nanostructure	Fabrication method	Resonance wavelength	Applications
Line	Interference lithography	446	RI sensing
	DVD technology	845	SERS
Thin film	Thermal evaporation	-	SEF
	Thermal evaporation	no clear	SEF
	Thermal evaporation	-	SEF
	Thermal evaporation	-	SERS
	Thermal evaporation	1.3- 2.5 eV	SERS
	Sputtering	400-550	PEC
AAO	Electrochemical anodization	-	SEF
	Electrochemical anodization	-	SERS
Hole	E-beam lithography	510	RI sensing
	Nanoimprint lithography (NIL)	550	RI sensing
	EBL	507	RI sensing
	Colloidal lithography	415	SEF
	Interference lithography	257	
Void	NIL	480	SERS
Concave	Electrochemical anodization	355	RI sensing
Triangular plate	NSL	508	RI sensing
Tapered cylinder	Extreme UV- IL	250	SERS
Bow tie	EBL	-	SERS

Table 1 summarizes the Aluminum plasmonic nanostructures, the fabrication methods and their analytical performances [43].

1.1.6. The application of plasmonic effect

1. Plasmon-enhanced catalytic reactions

The applications on the updating developments and applications in harvesting solar energy through plasmonic metallic nanostructures, mainly via two physical mechanisms: photothermal conversion and hot electron injection[45]. On the one hand, photothermal effect makes metallic nanostructures become nanoscale sources, which makes heat-generating for chemical reactions more easily-access; on the other hand, hot electrons from plasmonic metals present complicated influence on chemical

reactions, resulting to favorable bond cleavage or side effects among various reactions. Furthermore, this part will carry on investigating the potential application of local electromagnetic field enhancement. Further discussion of the mentioned effects are able to promote the designing efficiency, which aims to transfer solar light into chemical energy.

2. Designed Plasmonic Catalysts: Modified Au Nanostructures

Different implications have benefited from the study and research of photothermal conversion by Au nanostructures[46]. As it concludes, the management of size and shape is the adjustable characteristics of the plasmonic properties of Au nanostructures. Whereas, there is evidence proofing that Au nanocrystals have sensitive light reaction, especially compared to Au clusters, and the drawback of size burden impedes catalytic reaction activity. Thus, an influential inconsistency between plasmonic properties and reactive activities seems to exist to some extent. And under the light irradiation, as a necessary heat sources to boom the reaction temperature and time-limited requirement, Au nanocrystals play an important role. Consequently, it is favorable to carry out an approach to come across the drawback of Au nanocrystals, for example, by adjusting their features using catalytic metals such as Pd and Pt. Au substrates plays the role of light absorber, which acts to offer local heat; meanwhile the additive metals serve as the active sites[47].

Starting from the tip that Au nanorods adjusts Pd to obtain light energy in an organic catalytic reaction, which is shown in Figure 1.9 (a,b) [48], Yan and his team developed hybrid nanostructures to see the feasibility of generating heat in driving chemical reactions through photothermal conversion. On the basis of this argument, Huang's team synthesized Au Pd nanowheels for benzyl alcohol oxidation and Suzuki coupling reactions. Parallel methods are employed to get Pt-modified Au nanorods that show high activities in the production of nicotinamide adenine dinucleotide under light illumination as well, efficiently coupling solar energy into reactions.

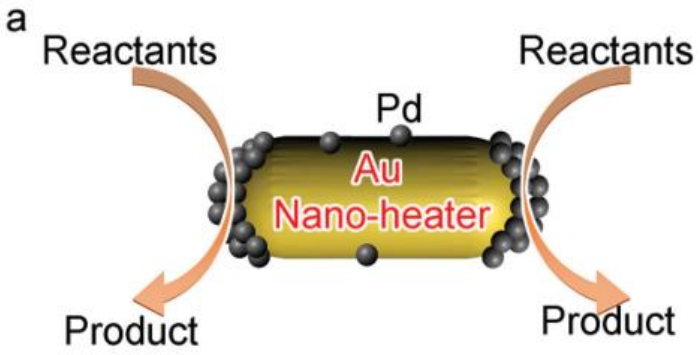

Figure 1.9. a) Schematic of Pd-tipped Au nanorods harvesting light energy for catalytic reactions[49].

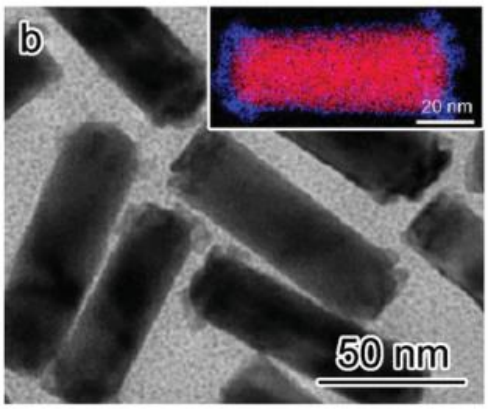

Figure 1.9. b) Transmission electron microscopy (TEM) and high-angle annular dark-field scanning transmission electron microscopy (HAADF-STEM) images of Pd-tipped Au nanorods[50].

3. Solar cells

As an environmental-friendly source with sustainability and low-harm, electricity transferred from solar energy via solar cell. The technology of solar cell is forecast to become a replacement of fossil fuel technique to satisfy the energy requirement all over the world. Great efforts of seeking for material and designing cell concept to enhance the efficiency and stability, to decrease the cost in the process of producing, installation and operating, make the cornerstone of success of solar cell technique. In thin-film solar cells, such as silicon-based and (organic polymer)-based ones, a main bottleneck in achieving high power conversion efficiencies is the trade-off among light absorption, photogeneration of electrons and holes, and charge-carrier collection at the electrodes. Effective light-trapping is an attractive approach to full absorption of incident sunlight, which is critical for achieving high power conversion efficiencies. In recent decades, light trapping strategies have been explored to increase the sunlight absorption in

different types of solar cells, including surface texturing, [51] use of photonic crystals, [52] and introduction of plasmonic metal nanocrystals [53]. Among these approaches, the use of plasmonic metal nanocrystals in solar cells has recently attracted much attention and been actively investigated [54].

Both lithgraphical fabrication and chemical preparation, relying on the kind of solar cell and related device structure, are able to incorporate with metal nancrystals. To be incorporated in solar cell devices, either directly embedded in solar cells or pre-attached on semi-conductor nanostructures, colloidal metal nanocrystals are chemically prepared [55]. For specific field like dye-sensitized solar cells, polymer solar cells, and organic/inorganic hybrid solar cells, colloidal metal nanocrystals and metal/semiconductor hybrid nanostructures are widely used due to its compatible with the device fabrication procedures of these types of solar cells. Embedding TiO_2 particles that are pre-attached with Ag nanoparticles in dye-sensitized solar cells has been demonstrated recently [56]. The loading of Ag nanoparticles increases the power conversion efficiency of the solar cells, with the enhancement factor depending on the loading amount of Ag nanoparticles (Figure 1.10 a). However, metal nanocrystals simply incorporated into solar cells are often easily corroded by liquid electrolytes. They also serve as recombination centers for photogenerated electrons and holes. [57] Coating of a SiO_2 layer on metal nanocrystals can partially overcome these problems. [58] Although a SiO_2 layer is able to protect metal nanocrystals from corrosion or other deleterious effects, SiO_2 is an insulator. It increases the resistance of the solar cells and therefore reduces the power conversion performance of the entire devices.

To cope with such issue, TiO_2 has been coated on (Au core)/(SiO_2 shell) nanostructures. [59] Since plasmon-enhanced electric field decays rapidly away from the metal surface, the use of the double shells increases the distance between metal nanocrystals and organic dye molecules and therefore degrades the enhancement effect. In this regard, direct coating of metal nanocrystals with TiO_2 becomes a promising approach to reducing the distance between metal nanocrystals and dye molecules, protecting metal nanocrystals from corrosion, maintaining a high electrical conductivity

of the active device material, and minimizing the charge-carrier recombination caused by metal nanocrystals. (Ag core)/ (TiO_2 shell) nanostructures have been prepared and introduced in the TiO_2 photoanodes of dye-sensitized solar cells. [60] The thin TiO_2 shell prevents photogenerated electrons from recombination with dye molecules and electrolyte species on the surface of Ag nanocrystals and improves the chemical stability of Ag nanocrystals. Figure 1.10 b shows the (photocurrent density)/voltage characteristics of the plasmon-enhanced and TiO_2 - only solar cells with the same photoanode thickness. A small amount of the (Ag core)/(TiO_2 shell) nanostructures (0.1 wt%) improves the power conversion efficiency from 7.8% to 9.0% while reducing the photoanode thickness by 25% for improved electron collection. The study implies that the plasmon-enhanced solar cells require 62% less material for maintaining the same power conversion efficiency as the conventional ones. The effect of the TiO_2 shell thickness on the enhancement for dye-sensitized solar cells has also been examined. [61] The nanostructures with a thin TiO_2 shell mainly increase the short-circuit current, whereas those with a thick TiO_2 shell improve the open-circuit voltage. Generally, the nanostructures with a thin TiO_2 shell produce the largest efficiency enhancement.

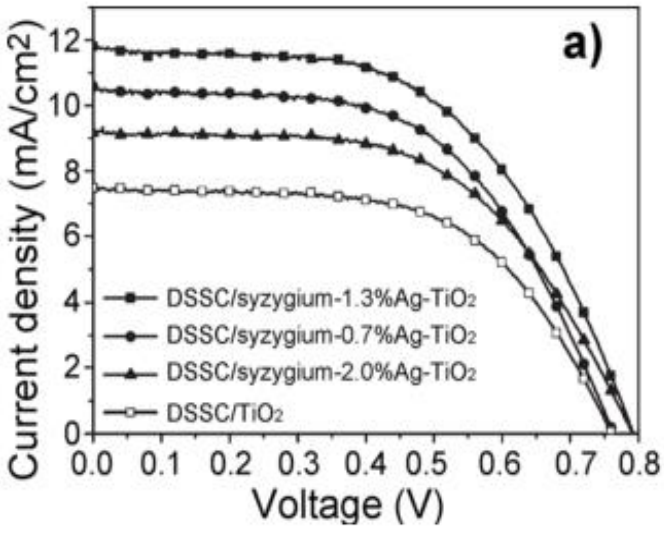

Figure 1.10. a) Curves of the current density versus voltage for the solar cells incorporated with Ag/TiO_2 nanostructures under AM 1.5 conditions (100 mW cm^{-2}) DSSC refers to dye-sensitized solar cell[62].

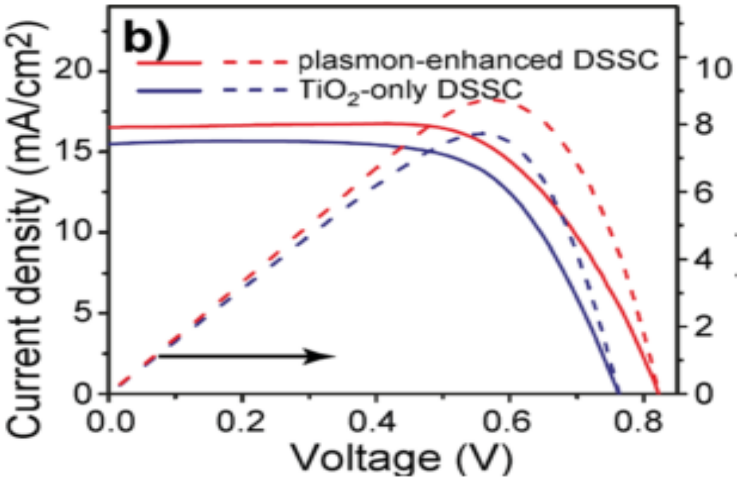

Figure 1.10. b) Current densities (solid lines, left axis) and power conversion efficiencies (dashed lines, right axis) of the solar cell containing Ag/TiO_2 nanostructures and the TiO_2-only solar cell[62].

1.2. Scope of the thesis

1.2.1. The research purpose

In this thesis, well-aligned TiO_2 nanotubes (TNTs) decorated with aluminum nanoparticles have been fabricated by electrochemical anodization and subsequently magnetron sputtering technique. UV-vis spectroscopy analysis indicate that photon absorption spectrum of crystallized TNTs with Aluminum nanoparticles is extended to visible light band with strong absorption (wavelength 400 – 800 nm). Photocurrent characteristics of the TNTs/Al show that the plasmonic nanoparticles Al contribute extra electron-hole pairs to enhance photocurrent under visible light illumination, which further indicate electrons generation, separation and transportation in this system. This thesis gives a systematic study of the subject for photon absorption enhancement of TiO2 nanotube arrays decorated with aluminum nanoparticles.

1.2.2. The research method

1. The fabrication of TNTs by anodization method. Research on the condition for anodization and decide the experimental parameter for the fabrication.

2. Rreactive magnetron sputtering system, called Sputter AJA 4050, deposited nanoparticles Al on the glass. The chamber pressure is set by 4.2mTorr, power by 120 W, gas by 10 scan, stable deposition rate by 0.4 Å/S. The dimension of nanoparticles Al have been calibrated on glass substrates with thickness from 0 to 20 nm, which can be controlled by the sputtering time.

3. Similarly, nanoparticles Al were deposited on titanium dioxide nanotubes. The dimension of nanoparticles Al have been calibrated on titanium dioxide with thickness ranging from 0 to 20 nm.

1.2.3. Outlines

Chapter 2 - Give background to the experiment part of the thesis where the fabrication set-up is presented and explained. The experimental method for characterization were used for acquisition of data are presented.

Chapter 3 - This chapter contains the introduction and application of TiO_2 nanotube arrays (TNTs) where the experimental procedure of fabrication of TNTs is presented and the methods used to analyze the morphology and electrochemical characteristics of TNTs are explained.

Chapter 4 - This chapter is related to photon absorption promotion of titanium dioxide nanotube arrays by metal of aluminum nanoparticles. The theory and experimental procedure of fabrication of decorated TNTs are presented. The methods used to analyze the morphology and electrochemical characteristics of aluminum decorated TNTs are explained. The affection of electrochemical characteristics for pristine decorated TNTs is discussed.

Chapter 5 - A short conclusion of the thesis and suggestions for future work are given in this chapter.

Chapter 2 Material and experimental background

The TNTs fabricated by anodization are different with the TNTs fabricated by other method, such as hydrothermal synthesis. With anodization, the top of TNTs is open, they are uniformed and highly ordered which are vertical to the side of the anodized Ti foil. In this way, the TNTs are with higher specific area and provide more rigid tubular channel path which means that anodization method is a promising method to make TNTs.

2.1 Material and experimental background

2.1.1. Materials

Chemicals and materials— Titanium foils (99.8% purity) were supplied by Baoji Titanium Industry Co., LTD and cut into the size of 30 mm×12 mm×0.3 mm. Ethylene glycol and ammonium fluoride (VWR International, LLC) were used as electrolyte for TiO_2 nanotubes preparation. Acetone, isopropanol and absolute alcohol were used for cleaning Ti foils and TNTs.

2.1.2. Anodization method

Before anodization, Ti foils were rinsed with acetone, isopropanol and DI water in ultrasonic bath (FinnSonicM12) for 15mins. After drying with nitrogen gas, the back side of Ti foil was covered with Scotch tape to prevent forming TNTs on the back side. The TNTs were fabricated by anodization of Ti foil in a fluoride-containing electrolyte solution, which consisted of 0.5 wt% ammonium fluoride (NH_4F), 97 vol% ethylene glycol (EG) and 3 vol% water. The anodization was performed in a double electrode cell with magnetic stirring under the constant potential of 60 V (VWR power supply

250 V) for 8 hours at room temperature (20°C). Ti foil (0.3 mm) and the thick Ti sheet (1 mm) was used as working electrode and counter electrode, respectively. A distance of only three center meters exists between the pair of electrodes. Following the process of anodization, they were rinsed by pure alcohol using the container of ultrasonic bath, or BRANSOIC 3510E-MTH, and this time period is required to last more than 20 minutes in order to remove the "grass-like" debris covered on TNTs [63]. Consequently, three hours of 500°C exposure in the air is prepared to form anatase TNTs.

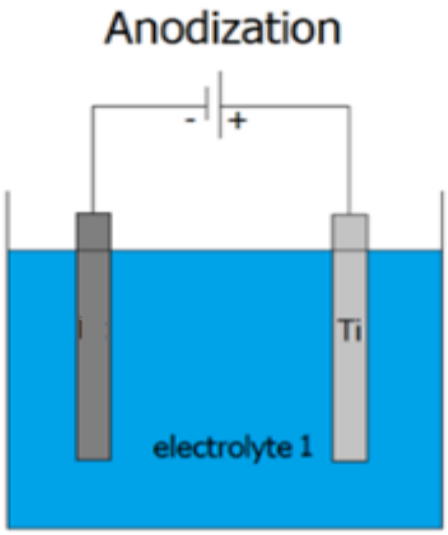

Figure 2.1: The anodization for TNTs

$$2Ti \rightarrow 2Ti^{4+} + 8e^{-} \quad (2.1)$$

$$Ti^{4+} + 4OH^{-} \rightarrow Ti(OH)_4 \quad (2.2)$$

$$Ti^{4+} + 2O^{2-} \rightarrow TiO_2 \quad (2.3)$$

$$Ti(OH)_4 \rightarrow TiO_2 + H_2O \quad (2.4)$$

$$8H^{+} + 8e^{-} \rightarrow 4H_2 \quad (2.5)$$

$$Ti + 2\,H_2O \rightarrow TiO_2 + 2H_2 \quad (2.6)$$

2.1.3. Sputtering method

Figure 2.2 (a,b)presents the procedure of the nanoparticles Al being deposited on TiO_2 nanotubes by a radio frequency (RF) reactive magnetron sputtering system, or Sputter AJA 4050.

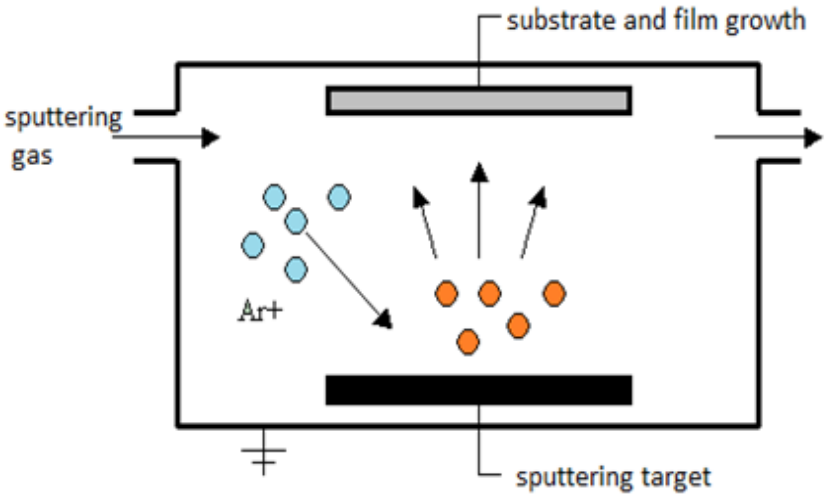

Fig.2.2(a) The procedure of sputtering[64]

Fig.2.2(b) Sputter AJA 4050

2.2. Characterization

2.2.1. Morphology

Morphology of the TNTs were characterized using scanning electron microscopy (SEM, SU8230) with an accelerating voltage 5 kV. X-ray analyzer (EDS) fitted to the SEM chamber was used to determine the composition. UV-vis light absorbance spectra were recorded by a UV-vis spectrophotometer (SHIMADZU, UV-2600 with ISR-2600 Integrating Sphere Attachment) with fine $BaSO_4$ powder as reference in the range of 220~800 nm. Photocurrent performance and response of Al/TNTs were evaluated with an electrochemical workstation (Zahner elektrik IM6) in two-electrode configuration.

2.2.1.1. Scanning electron microscopy

A scanning electron microscope (SEM, SU8230) is a type of electron microscope that produces images of a sample by scanning the surface with a focused beam of electrons (Fig 2.3). The electrons interact with atoms in the sample, producing various signals that contain information about the sample's surface topography and composition. The electron beam is scanned in a raster scan pattern, and the beam's position is combined with the detected signal to produce an image. Specimens can be observed in high vacuum in conventional SEM, or in low vacuum or wet conditions in variable pressure or environmental SEM, and at a wide range of cryogenic or elevated temperatures with specialized instruments. [65]

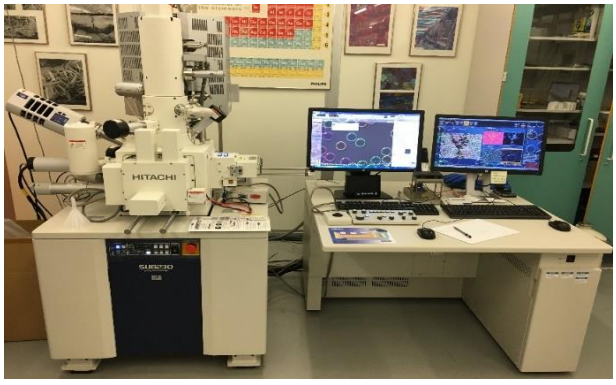

Fig 2.3. SEM, SU8230

2.2.1.2. X-ray analyzer (EDS)

EDS is an analytical technique used for the elemental analysis or chemical characterization of a sample. It relies on an interaction of some source of X ray excitation and a sample. Its characterization capabilities are due in large part to the fundamental principle that each element has a uniqueatomic structure allowing a unique set of peaks on its electromagnetic emission spectrum, EDS is shown in the figure 2.4.

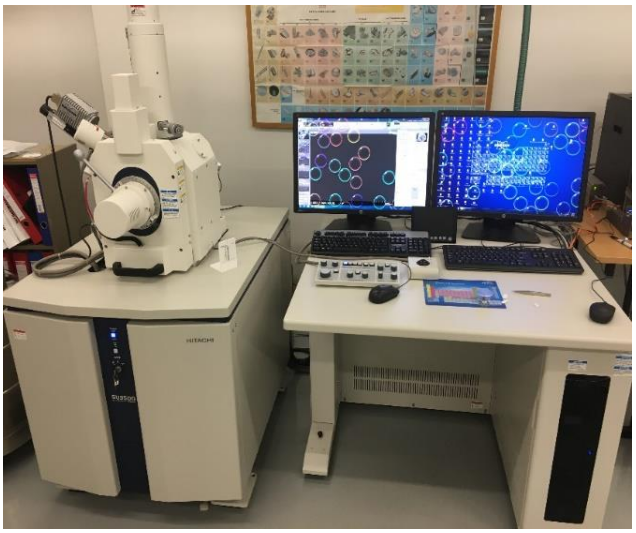

Fig 2.4. SEM, SU3500

2.2.1.3. UV-vis spectrophotometer

Ultraviolet–visible spectroscopy (SHIMADZU, UV-2600 with ISR-2600 Integrating Sphere Attachment) or ultraviolet-visible spectrophotometry (Figure 2.5) refers to absorption spectroscopy or reflectance spectroscopy in the ultraviolet-visible spectral region. This means it uses light in the visible and adjacent ranges. The absorption or reflectance in the visible range directly affects the perceived color of the chemicals involved. In this region of the electromagnetic spectrum, atoms and molecules undergo electronic transitions. Absorption spectroscopy is complementary to fluorescence spectroscopy, in that fluorescence deals with transitions from the excited state to the ground state, while absorption measures transitions from the ground state to the excited state. [66]

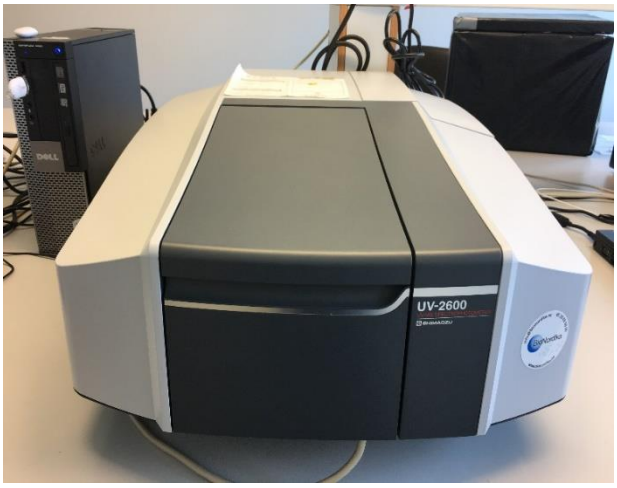

Fig 2.5 SHIMADZU, UV-2600

2.2.2. Electrochemical characteristics

The electrochemical characteristics of the samples were evaluated with electrochemical workstation (Zahner elektrik IM6 shown in Figure 2.6) in a three-electrode configuration shown in Figure 2.7. The electrochemical experiments for TNTs were carried out in 0.5M Na_2SO_4 aqueous solution, where Ag/AgCI (3M KCI) electrode was used as reference electrode and a plantinum wire as counter electrode. The experiments include Cyclic voltammertry(CV) test.

Figure 2.6: electrochemical workstation (Zahner elektrik IM6).

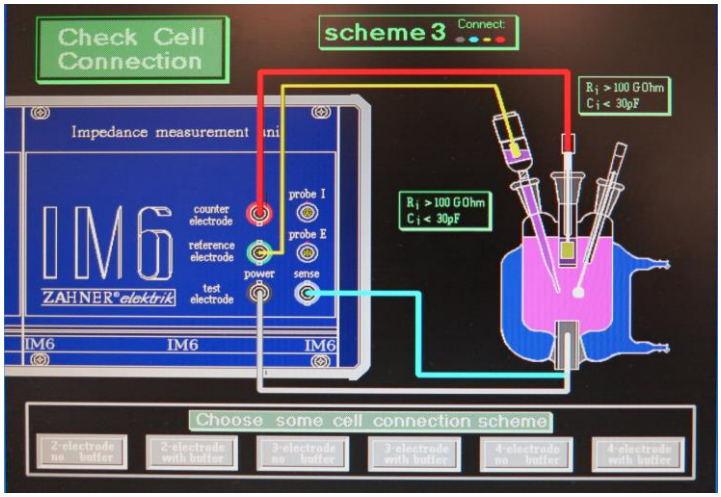

Figure 2.7: A three-electrode configuration

2.2.2.1. Cyclic voltammertry (CV)

As a generally-accepted potentiodynamic electrochemical measurement, Cyclic voltammetry (CV) is highly-appealed. In an experiment using cyclic voltammetry (Fig 2.8), the potential of working electrode is ramped linearly related with time. Different from linear sweep voltammetry, following the process of setting a favorable potential in a CV experiment, there is an opposite trend between the working electrode's potential and the original one. And it is reasonable to repeat the cycles of ramps in potential as more as possible. These may be repeated as many times as needed. The current at the working electrode is captured versus the applied voltage, or the working electrode's potential to give the cyclic voltammogram trace. To investigate the electrochemical properties of an analyte in solution [67], it is meaningful to carry on cyclic voltammetry. In a variety of chemical field, electroanalytical technique applying cyclic voltammetry has produced huge attraction, which is applied to explore the process of redox in testing the stability of reaction products, the existence of intermediates [68], electron transfer kinetics [69], and the reversibility of a reaction [70]. Aiming to test the systemic electron stoichiometry, required identification tool includes diffusion coefficient of an analyte and the related formal reduction potential. Besides, since that current in a reversible, Nernstian system has integrated considerable amount of attraction, the

attraction of an uncertain solution is carried out due to the aggregation of a calibration curve of current vs. Attraction. In the field of cellular biology, living creators are used to measure such attractions. Whereas in the field of organometallic chemistry, it is used to estimate redox mechanisms. [71]

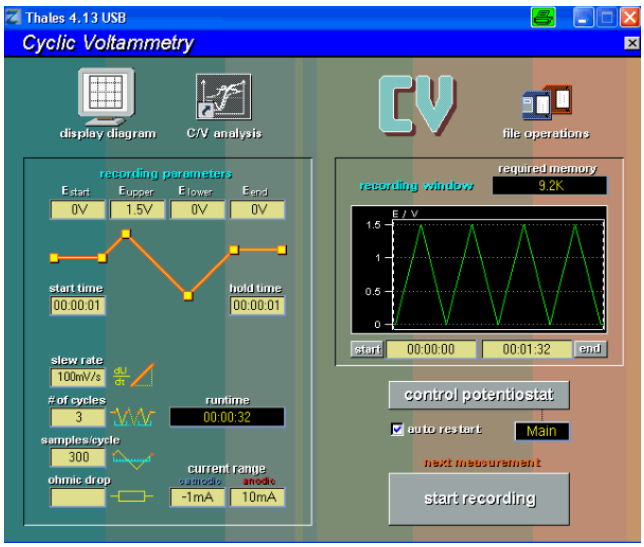

Figure 2.8: The data setting of CV tests

2.2.2.2.Electrochemical impedance spectroscopy

Electrochemical impedance spectroscopy (Figure 0.9) is one of the techniques, which has been used to evaluate the electrodes performance. Electrochemical impedance is the response of the electrochemical system to an applied potential, the frequency dependence of this impedance can reveal underlying chemical processes. The response of electrochemical systems is very non-linear; the complex response of the system is usually displayed in Nyquist format using the frequency range from higher to lower. For an ideal supercapacitor, the Nyquist plot should be one straight without changing to the frequency, there is a well defined semi-circle region at the high frequency range, and a straight line which is almost vertical appears at a low frequency range, these are the characteristics of ideal capacitors. The diameter of the semi-circle represents the interfacial charge transfer of faradic resistance. [72]

2.2.2.3.Current-voltage (I-V) characteristics

Cyclic voltammetry is a very widely used technique for the interrogation of physics and chemistry at the interface between an electrode and an electrolyte, such as a saline solution, in which the current is plotted against the voltage applied to an electrochemical cell. The voltage is swept up and down across a range of values to successively drive the opposite directions of an electrolysis reaction. we always want to maximize our current in order to maximize sensitivity, so this analysis can help in practical design of the electrochemical cell and chemical environment. Comparison of predicted and measured voltammograms enables determination of material properties and other system parameters that may be unknown, such as diffusion coefficientsand reaction rates. [73]

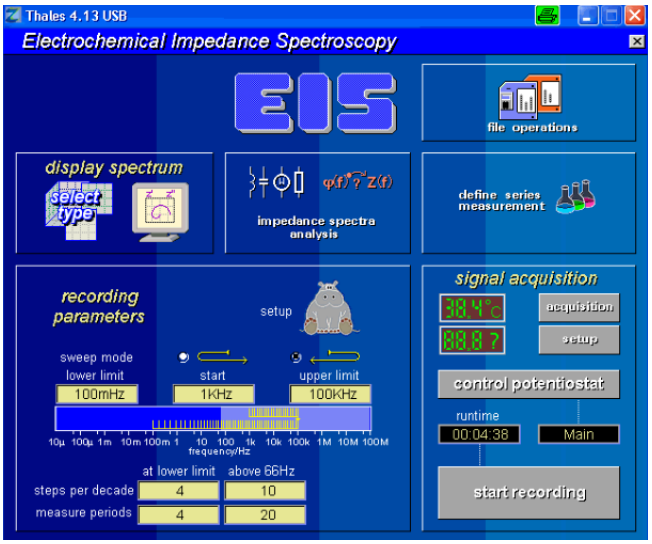

Figure 2.9: The data setting of EIS tests

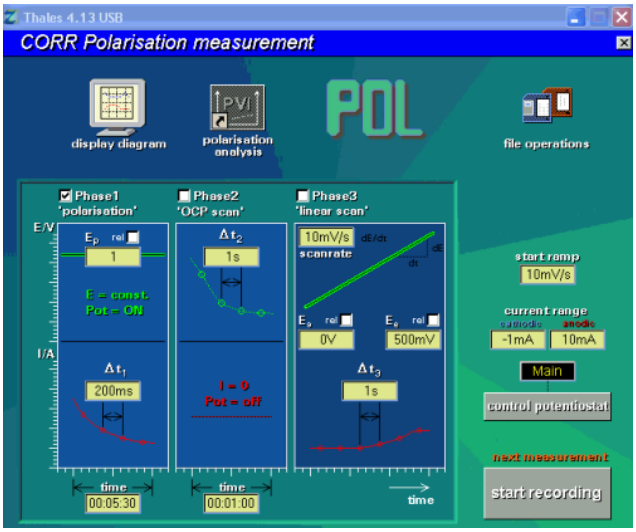

Fig 2.10 The data setting of I-V tests

Chapter 3 Pristine TiO_2 nanotubes Arrays

3.1. Introduction of Titanium dioxide nanotubes

Lijima's discovery of carbon nanotubes inspired the field of nanotechnology and triggered enormous efforts in physics, chemistry, and materials science, due to the combination of extreme molecular geometry and exciting properties. These aspects of nanostructures (1D) provide a unique feature, such as electronic flow electrons or the effect of quantum closure of a waste surface area is very high, even with a high mechanical power[74]. Despite the prospect and stockpile of solid carbon nanotubes, it is important to note that sulfides and transition metal are fully controlled, but synthesized in a (1D nanowires geometry 1D, Nanofibers, however, nanorods nanometer) with chemical properties and fascinating new attitudes.Multi-polarization and carbon nano should attract attention to microelectronic use, especially nanotechnology, inorganic sulfides metal, is the golden metal material-specific fabricated to other record residents of the property, and the studies on software, solicit letter of intent are applied in the field of biomedical photochemical[75], electronics and environment.In all metals oxides, transition-metal TiO_2 is extensively made of fluorine, using more than 40000 publication well prepared material over the previous decade. Thus capable of TiO_2 to this should be compound in materials science[76]. Bulk TiO_2 is treated as the useful non-toxic, environmentally friendly, corrosion-resistant material due to its utility in white paint, paint, sun-blockers etc. Apart from medicinal utility in biocompatibility and special ionic and electronic oxide properties, the main functional characteristics are highly appealed[77]. Especially in the form of TiO_2 crystal, the wide-bandgap semiconductor with suitable band-edge positions enables its utility in solar cells and for photocatalytic reactions. In the application of transferring splitting water into oxygen and hydrogen, which is treated as the prospective fuel, or the application of hazardous waste remediation, like the polluted ground water or the toxic air management, photo-generated electron– hole pairs play essential role[78]. In the last

two decades, devices on the basic of sophisticated photovoltaic, electrochromic, antifogging, or self-cleaning properties, biomedical coatings, sensors, or smart-surface coatings [79] are established. Among most of the applications, the area of special surface, such as the catalytic reaction should be seriously maximized in order to reach the top general efficiency. Thus, TiO_2 in the form of nonparticulate is generally applied.

3.2. The fabrication methods of TiO_2 nanotubes

The main fabrication of TiO_2 nanotubes include: firstly, in a certain concentration of alkaline solution, the hydrothermal synthesis of TiO_2 nanoparticles. Second, preparation of TiO_2 nanotubes by anodic oxidation of Ti foils.

(1) Hydrothermal synthesis

In a typical hydrothermal synthesis, TiO_2 nanoparticles are dissolved in a concentrated alkaline solution to form a mixture, after moving into an autoclave at a hydrothermal temperature range of 110 ^oC to 150 ^oC, the mixture can be converted to a nano-size crystallized tubular titanate structure, then washing the resulting materials with dilute acidic aqueous solution or solvents such as water, a final TNT products can be achieved [80]. The entire synthesis is simple and cheap which is good to be industrialization. Zhang et al. [81] got the titanate by hydrothermal synthesis, then by the H+ and Na+ exchange and calcinations, they got the length of 200nm and diameter of 6~20nm TNTs. But in this way, usually the TNTs are disordered and interwined [82]. Tian et al. [83] deposited one layer of TiO_2 nanoparticles on the titanium sheet, put it in the 10mol/L NaOH solution, after calcintion at 160^oC, one layer of ordered TNTs film can be achieved. The typical process flow is shown in Figure[84].

(2) Anodic Titanium Nanotubes

Hydrothermal synthesis [86] and the process of templated sol-gel [87] cover the nanotube preparation. As early as 1920s, nanoporous structure of anodized Ti metal was studied in academic field. Zwilling et al. [88] study argued that acting as the electrolyte and aiming to perform the titanium anodization and the related alloy (TA6V), especially at the moment of chromium acid in utility, a compact oxide film was obtained;

whereas in an HF/chromium acidic electrolyte, a nanoporous structure was obtained instead. At the beginning of 21 centuries, Grimes et al. carried out a systematic study on the nanotubular structures for the process of titanium anodization, which has generated hot attention on the setup of the related theory of growth model, crystal structure and so on. At the same time, huge amount of functional devices have been investigated and established on the basic of the nanostructures[89].

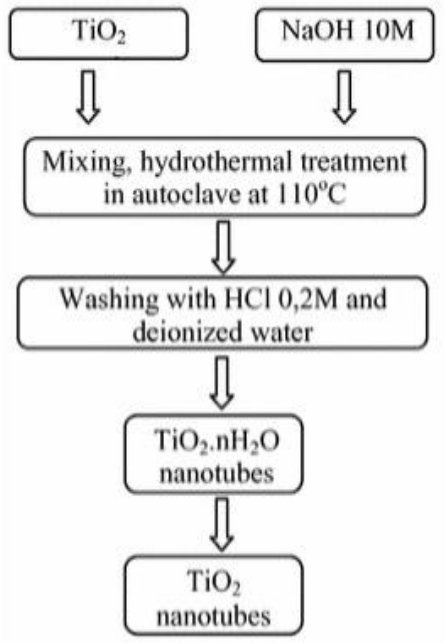

Figure 3.1. Diagrams of hydrothermal synthesis of TNTs[85]

This section will further investigate the developing process of anodic titanium nanostructures. Related experimental data gives out the suggestion that electrolyte kinds, anodizing potential, processing temperature, reaction time, as the main characteristics, influence the overall nanostructures. The following part will present in detail.

(3) HF Acid-Based Anodization

Due to the fact that HF owns the most efficient for the anodization of titanium, it is generally applied as the electrolyte and the corresponding patameters have been researched and optimized. The study of Gong et al. [90] concluded that with an HF of 0.5 wt%, a nanoporous structure was obtained at a relatively low anodizing potential (<3 V) while discrete nanotubular arrays were obtained when the potential 5 V. As the potential anodization raises to more than 40 V, it is reasonable to capture randomly

distributed pores due to the deterioration of the nanotube structure. Their study revealed the suggestion that nanotube formation in the horizon of selected electrochemical window ranges from 10 V to 40 V, which intensively showed high sensitivity to electrolyte concentration and applying capability. Moreover, they found that there is a positive relationship between the factor of diameter, wall thickness, nanotubes length and anodizing potentials[91].

Similar report of anodization experiments investigated HF contained mixture electrolytes. Like Macak et al. [92], which reported that adjusting anodization to the oxalic acid/0.5 wt% HF (1:7 in volume ratio), the captured nanotube could not present dramatic difference in diameter and shape except for wall thickening. When anodization was set at 10 V, the inner diameters of the nanotubes reached at about 20 nm, and the wall thicknesses stood at ~15 nm. Deeper analysis told the fact that the wall thickness and the tube length are both influential function of anodizing temperature. While decreasing such temperature, based on low dissolution rate, the wall thickness increases, resulting to a big plump between the interspace of neighboring nanotubes which connects the nanotubes and finally forms a nanoporous structure. This experiment gives evidence that, in the process of anodization, chemical dissolution and electrochemical etching are the two main independent factors.

The study of Beranek et al. [93] investigated the process of anodization in H_2SO_4/HF electrolyte. In their conclusion, in the electrolyte of H_2SO_4, anodization shows good performance, as long as anodic current goes smoothly. Whereas successive oscillation happens, and the range remains integrated. They attempted to analyze such phenomenon by the competition between oxide formation and dissolution, among which HF acts as the main feature in the generation of oxide layer dissolution. At the end, this competition produces a limitation of length, especially at the time of nanotubes being fabricated in HF contained electrolytes. The interrelation between nanotube length and the above explained competition of oxide formation and dissolution is an attractive researching topic in the academic field. Scholars also looked into the oscillation of anodizing trend, however, a consistent argument is hardly reached.

(4) Neutral Electrolyte-Based Anodization

As the above section explained, Beranek's study of the correlation between nanotube length limitation and growth mechanism remained attractive in the academic field. The similar argument was agreed by Macak et al. [94,95] and Bauer [96]. Macak et al. study insisted that length limitation is in reality among thousands of nanometers, especially at the time of anodization being performed in the horizon of HF-based electrolytes. Such length limitation stems from the dissolution due to the surface of acidic electrolyte. Consequently, aiming to gather nanotubes of high aspect ration (L/D), both the highest and the lowest dissolution rate of nanotubes are expected to be adjusted, which stands for the fact that the lowest nanotube formation rate has a negative relation between the highest nanotube dissolution. These scholars came up with this idea under the inspiration of employing neutral electrolyte, while they also gather the huge aspect ration of nanotubes. The selected experimental neutral buffered electrolytes were $NH_4F/(NH_4)_2SO_4$[97] and NaF/Na_2SO_4[98]. Via the attempt of neutral electrolyte application to increase the growing rate, a relative low pH value was set up at the bottom of the nanotube; whereas in the opposite side, at the top or in the wall area of the nanotube, a relative high pH value effectively prevented the process of electrochemical dissolution. Therefore, the researchers successfully achieved the second generation of nanotube, which keeps array with huge aspect ratio. Macak study regulated the electrolyte pH value in various attempt of significant level, which are confirmed to be significant.

Grimes et al. [99] carried out another study of Anodic titanium nanotube with the length of a large amount of micron meters, especially controlling the anodization in a KF, or NaF electrolyte. Based on their empirical results, pH value is statistical significance on electrochemical dissolution in the process of anodization. This statistical significance stems from hydrolysis of titanium ions. Under normal conditions, nanotubes with long length can formed as the pH value of the electrolyte remain less than seven in a relative high level. For a fixed pH value, there is a positive relation

between the length & diameter and the anodization potential. While for a fixed anodization potential, the diameter does not show statistical significance to pH value.

In another study by Cai et al. [100], empirical evidence showed that the extension of anodizing time is not positively related to the nanotubes length, especially when pH value is set to less than 1. In reality of a weak acidic electrolyte, the nantube length is significantly positively related to anodizing time. They gave out evidence shows that a pH value ranging from three to five provides a favorable environment to get nanotubes with large aspect ratio. The feature of short but clean is defined as the the characteristic of nanotubes forming in an electrolyte with a low pH. Correspondingly, a high pH contributes to the set up of nanotubes with long length. When the mouth of nanotubes is opened, intensive coverage usually occurs and alkaline electrolytes can not provide a good environment to form nanotubular structure. Cai et al.'s work implies systematic influence of pH environment on nanostructure morphologies. They insisted that nanotube growth highly relies on the competition between formation and dissolution of oxide layer, furthermore, they insisted the role of the length of tubes at the same time.

Scholars like Macak et al. [101] found the importance of regular strips on the outer wall of nanotubes, and they further ascribed such strips to the current oscillations. So did the study in Richter et al. [102]. They reached an agreement that by controlling the anodizing time via the length of tube, there is a perfect match between the oscillation frequency and adjacent strip distance. On the basic of this argument, it is suggested that the original cause of current oscillation and final strips formation both stem from the pH value fluctuation. Thus, instead of the traditional electrolyte, the scholars utilized high-viscosity electrolyte to adjust the pH value. Under this condition, the nanotubes with smooth walls were perfectly ready.

(5) Anodization in Organic Electrolyte-Based

As the Ti anodization techniques become more popular, various electrolytes were studied to assess the nanostructure morphologies. The utility of electrolytes is not consistent with the limitation from the traditional aqueous solutions, but with multiple choices to organic solutions. Different from the former investigated nanostructures,

Tsuchiya et al. [103] gave out a titanium nanotube arraying with “coral reefs” morphology, which were fabricated at high anodizing potential in F-contained “water-free” acetic acid electrolyte. Anyway, there was still an absent explanation of the effect as why the using of acetic acid may result in such a nanostructure.

The study of Ruan et al. [104] gathered highly ordered nanotube arrays at the time of anodization performing in an HF-contained dimethylsulfoxide (DMSO)/ethanol mixture electrolyte. Based on their study, the nanotubes gathered an electrolyte presenting an intensive photoelectric response, comparing with that formed in conventional aqueous electrolytes. The special morphologies ascrib advanced properties. But the correlation between the electrolyte and the morphology still requires further investigation.

(6) Template-assisted method

For the template-assisted method, titanium dioxide nanotubes are formed in vertically aligned structures on a thin film material by aiding of tubular-like structure as templates for formation of tube pillar. For example, the nanotube structures of the titanium dioxide were grown using a chemical vapor deposition (CVD) system as reported by Mustafa Karaman [105] in which the TiO2 nanotubes were produced via the template-assisted method by depositing titanium dioxide thin films onto electrospun polymethyl methacrylate (PMMA) fibers via the hot-filament chemical vapor deposition method. Lee et al. [106] successfully fabricated zero-cracked titanium dioxide nanotubes in a highly-ordered arrangement using the atomic layer deposition (ALD) method and anodic aluminum oxide (AAO) as a template. However, TiO_2 nanotubes were also successfully fabricated using ZnO nanorods as a template and were deposited onto indium-doped tin oxide (ITO) [107] and fluorine-doped SnO_2 transparent conducting glass oxide [108]. Besides, Chien et al. [109] had successful fabricated TNT by using anodic aluminum oxides (AAO) templates with diameter of 200–500 nm. The light and transparent AAO make it favorable as the TNT template plus with strong mechanical strength and high flexibility. Direct growth of TNT was investigated on plastic substrate and the result gave an outstanding performance in gas sensoring properties.

(7) Sol-gel method

The sol-gel method is typically used in conjunction with another process, such as the template-assisted method or the hydrothermal method, until the TiO_2 nanotube fabrication process is complete. Based on Liu et al. [110], ZnO nanorods were used as a template to create TiO_2 nanotubes using the sol-gel process. Pang et al. [111] successfully fabricated TiO_2 nanotubes via the sol-gel method, followed by the hydrothermal method. The product from the literature [111] was also used during the sonocatalytic degradation of Rhodamine B in aqueous solution. Camposeco et al. reported the production of TiO_2 nanocrystals using the sol-gel method, followed by the hydrothermal method, to generate TiO_2 nanotubes. Titanium butoxide was used as a precursor and mixed with butanol to create a gel that was dried at 80 °C for 12 h. From these studies, it was discovered that the surface area, pore volume and pore diameter of the nanotubes obtained via the hydrothermal method were marginally higher than the nanocrystals obtained after the sol-gel process.

3.3 The influence factors of formation of TNTs

The factors that can affect the formation of TNTs by anodization are related to the anodizing voltage, the electrolyte, the PH and the anodizing time.

(1) Anodizing voltage

The anodizing voltage is the main factor of the diameter control of the TNTs. In general, the higher the voltage, the bigger the diameter of TNTs and the longer the length of TNTs. The lower the voltage, the smaller the diameter and the shorter the length of TNTs. However, when the voltage is too small, it is impossible to form the nanotube structure, on the opposite, when the voltage is too big, it will form the spongiform randomized porous structure, when the voltage reach one value, the Ti foil will be corroded, there will be no TNTs [112]. When the voltage increases linearly, it will form the conical-shaped TNTs [113].

(2) The PH of the electrolyte

The dissolution rate of TiO_2 affected a lot by the PH of the electrolyte [114]. The research shows H+ will help F- dissolve TiO_2. In order to limit the dissolution of TiO_2, the concentration of H+ should be decreased, control the PH of electrolyte. Some people put buffer solution in the electrolyte to adjust the PH and fabricated TNTs, the result is good [115].

(3) Anodizing time

At the beginning of anodization of Ti foil, when the time increase, the length of TNTs will increase, until the rate of oxidation of Ti foil and the rate of dissolution of TiO_2 are equal, the length of TNTs will not increase. Many tests should be made to find the right anodizing time.

(4) The composition of the electrolyte

For the anodization, the properties affect a lot the oxidation of Ti and the dissolution of TiO_2. Three factors should be paid attention to choose the right electrolyte: first, HF electrolyte and or acid HF mixed electrolyte [116], since the TiO_2 dissolve fast in HF electrolyte, the length of TNTs will be only 500nm. Second, for the neutral NaF and NH4F buffer electrolyte [117], the length of TNTs can reach um, the specific surface area can reach 50, but the walls of TNTs can be a little rough. Third, for the organic electrolyte containing F-, such as glycerol and Vinyl alcohol are the most promising electrolyte.

3.4. The anodization method of highly ordered TNTs

In this thesis, the TNTs were fabricated by anodization of Ti foil in a fluoride containin gelectrolyte solution, which consisted of 0.5 wt% ammonium fluoride (NH4F), 97vol% ethylene glycol (EG) and 3vol% water [118]. TNT arrays were fabricated using electrochemical anodization technique in a two-electrode system with magnetic stirring under the constant potential of 60 V (VWR power supply 250 V) for 1h at room temperature (25°C). Ti foil was used as working electrode and the Ti sheet foil (30 mm×12 mm×0.3 mm) was used as counter electrode. The distance between two electrodes is 3 cm. After anodization, they were rinsed with absolute alcohol in a mild

ultrasonic bath (BRANSOIC 3510E-MTH) for 15 mins to get rid of nano fibrous debris covered on the surface of TNTs [120]. The cleaned membranes is left to dry in air with the anodized surface facing up. Then the as prepared amorphous TNT arrays were annealed at 400°C (LENTON WHT6) for 2 hours in air to form anatase TNTs. The fabrication of TNTs is shown in Figure 3.1.

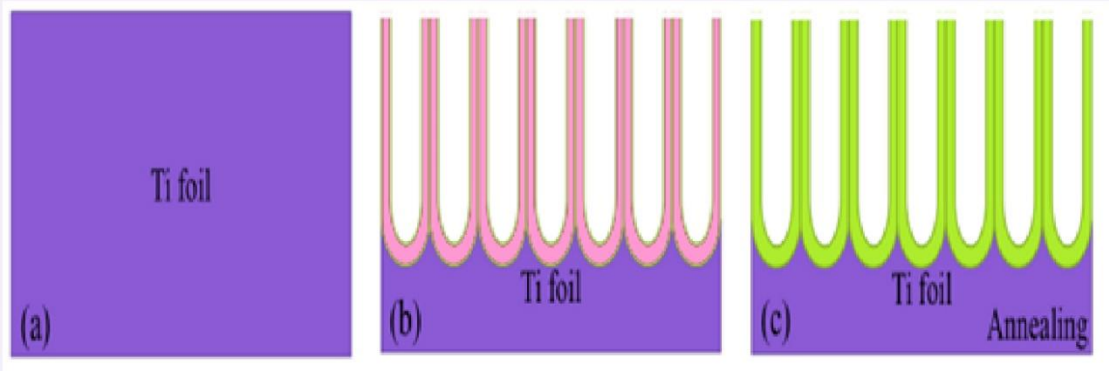

Figure 3.2. The fabrication process of TNTs

3.4.1. Results and discussion

3.4.1.1. SEM measurement

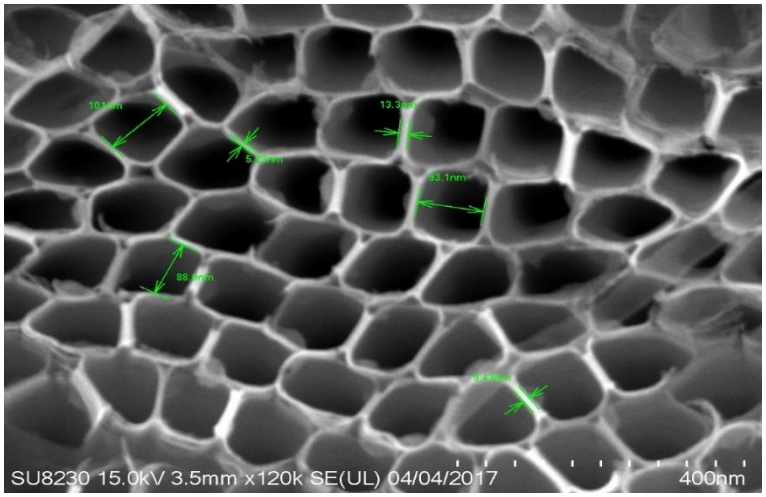

Figure 3.3: Top-view SEM images of TNT

Figure 3.2 shows the surface and cross-sectional morphology of the TiO_2 nanotubes, close-packed nanotube topography was obtained on Ti surface after anodization, each individual nanotube is composed of numerous TiO_2 grains that are close packing. The prepared sample were clearly observed a periodically porous structure with an average diameter of ~90 nm and a wall thickness of ~9 nm.

3.4.1.2. UV-vis spectroscopy analysis

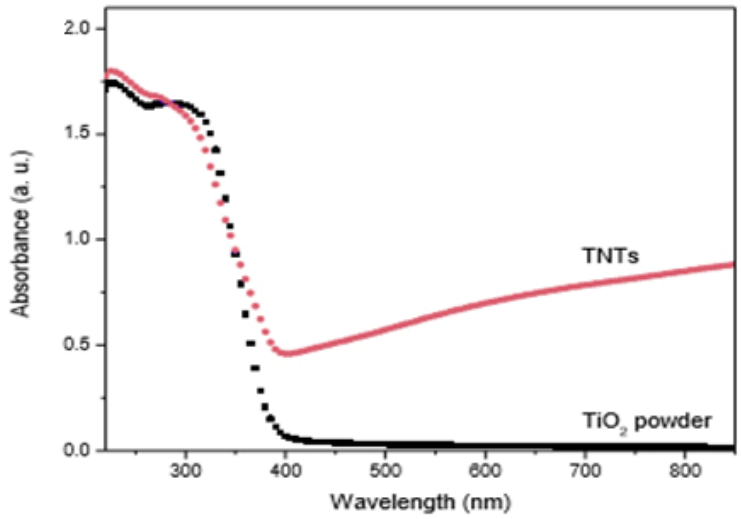

Figure 3.4: The absorption spectra of TiO_2 powder, pristine TNT arrays and prepared at 60V/1h.

The absorption spectra of TiO_2 powder and pristine TNT arrays are showed in Figure 3.3. The TiO_2 powder has extremely weak absorption of visible light at the wavelength above 400 nm which is almost zero. For TNT arrays, the absorptive spectra increases at the visible light region from 400 nm to 800 nm. Therefore, TNTs are much better visible light harvesting material than TiO_2 powder.

3.4.1.3. The electrochemical characteristics of TNTs

Under the exposure of white light by on-off cycles, the measure of photocurrent reaction was conducted. At the time of light being turned on, photocurrent suddenly peaks; and an instantaneous recovery to the beginning value occurs when the white light disappears. Figure 3.4 compares the CV response for TNTs electrode prepared at 60V/6h, 60V/12h and 60V/16h at a scan rate of $50mVs^{-1}$. The CV curve of TiO_2 prepared at 60V/16h exhibits the highest responsive photocurrent compare to TiO_2 electrodes prepared with 60V/12h and 60V/6h, the anodization time of fabrication of TNTs increase, when integrated area of CV curves increase, illustrating an enhanced photocurrent. The reason for the improvement can be that the TiO_2 prepared at 60V/16h has biggest

specific surface area than TiO_2 prepared at 60V/6h and 60V/12h. The bigger specific surface area, the higher responsive photocurrent.

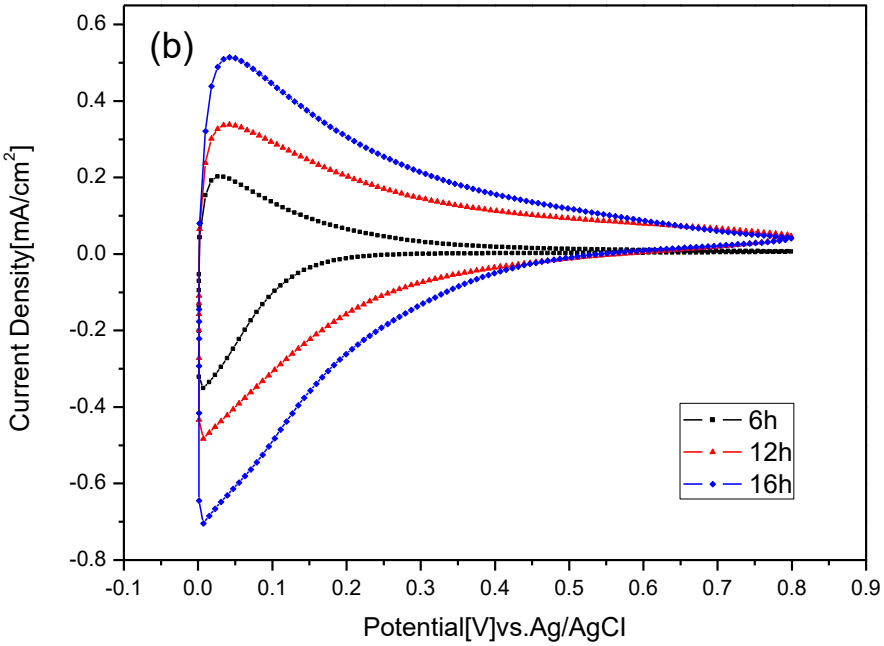

Figure 3.5: CV curves collected at 50mVs^{-1} for 60V/6h, 60V/12h and 60V/16h TiO_2.

3.5. The application of TNTs arrays

To understand the TiO_2 nanostructure application, it is required to firstly exploit the special feature of TiO_2, for example, the electronic, ionic, or biocompatibility properties can be treated as potential starting points. Similarly, to effectively increase the rates of reactions or transport, employing small scale dimensions, for instance, large surface area, short diffusion path, or size confinement effects, plays an essential role. In addition, nanotubular assemblies also helps to enhance the systemically dimensionality. Tubes grown on a metal substrate are vertically aligned to a back contact; in other words, a direction for charge transfer towards the electrode is established. By offering a well-defined top openings, Nanotube layers are thus suitable for size-selective applications (filters) or for templating secondary material. Since that inside volume is well-defined and regular, applications, such as nano test tubes [121] are promising. In the following

section, an overview of current efforts towards TiO_2 nanotube applications are discussed in detail.

(1) TiO_2 Nanotube Arrays: Application to Hydrogen Sensing

This section focuses on the TiO_2 nanotube application in the area of hydrogen gas sensing. As early as 2003, Varghese et al. [122] demonstrated hydrogen sensing in the environment of quite high temperature, using TiO_2 nanotube arrays several hundreds of nm in length, anodized in HF aqueous electrolytes [123]. Since that time, scholars realized that based on the absorption of molecular hydrogen, the sensitivity between the electrical resistance of the TiO_2 nanotubes and hydrogen, and such sensitivity is completely reversible. For instance, a tube with pore size of seventy-six nm, a deviation exists in the evaluated resistance of 10^3 upon exposure to 500 ppm hydrogen at 290 °C. The paper suggested that the sensitivity between the hydrogen and nanotubes was considerably related to nanotube diameter, with 22 nm pore size nanotubes being about 200 times more sensitive than 76 nm pore size nanotubes, although the smaller pore size nanotubes have a larger surface area by only 30%. Different kinds of hydrogen sensor technologies [124], like Schottky junction [125], fiber optic [126], catalytic [127], electrochemical [128], field effect transistor (FET) [129], oxide semiconductor [130] and combinations of the above as well, have already been researched and developed, or would be further investigated in the near future. Oxide semiconductor gas sensors are relatively simple and inexpensive as well. Anyway, they are previously carried out at favorable temperatures, especially increasing the temperature to hundreds of Celsius to promote the gas sensitivity and to prepare condition for fast and reversible reactions. But actually, adjusting temperatures are not feasible in wide applications, like those relating to flammable environments, biomedical applications, and those requiring low-power operation. The literature [131] shows little efforts in hydrogen sensing at room temperature. A key issue with any sensor platform is the potential for unnecessary contamination, or poisoning, which usually introduces faked-measurements and ends its useful life. A sensor for an uncontrolled environment is facing potential contamination, for instance, from volatile organic gases. The huge advantage of sensor

technology is being able to self-clean, which largely extend the working lifetime and reduce the possibility of faked measurement. And finally, the limitation of contamination is handled by ultraviolet (UV) illumination of the nanotube array surface [132]. Titanium dioxide is a semiconductor, which is characterized by a filling of the valence band and an empty conduction band. At the time of bandgap energy being surpassed by photon, an electron – hole pair are produced. As the oxidants, valence band holes are suggested to be powerful, while conduction band electrons act as outstanding reducers. Most organic photodegradation reactions utilize the oxidizing power of electron holes, either directly or indirectly, producing carbon dioxide and water without production of potentially toxic side products [133]. There are four frequently-mentioned factors doing good to improve photocatalytic efficiency. Firstly, the existence of electron-hole pairs on the surface; secondly, longer electron-hole recombination lifetimes; thirdly, geometries providing higher surface-to-volume ratios; and fourthly, a predominance of the anatase crystalline phase. The front three factors are directly have direct link with the material architecture [134], while the forth one is adjusted via subsequent annealing of the initially amorphous nanotubes. At room temperature, TiO_2 nanotube array hydrogen sensors were applied to demonstrate the self-cleaning ability. Their photocatalytic properties resulted from the fact that the hydrogen-sensing capabilities of the sensors are largely recovered by UV light exposure after being completely extinguished by the rather extreme means of sensor contamination: coating the sensor using motor oil. Metal oxide semiconductors are not able to give exact respond to a particular gas from a mixture. Thus at this time, chemical modification, such as doping or surface functionalization, is highly required [135]. Under the help of nanotechnology, a lot of nanostructures of functional metal oxides are studied for environmental sensing. And it has already turned out that nanoscale architectural features show ideal performance by over-performing gas-dependent electrical behavior [136]. Titanium dioxide nanotubes arraying of up to a few microns in length, pore diameters ranging from 22 nm to 110 nm, and wall thicknesses ranging from 9nm to 34 nm show an unpredicted change in electrical resistance in response to

low levels of hydrogen at room temperature. Empirical data reveals that nanodimensional structures own outstanding properties that micro/macroscale structures can never exhibited, which has the potential to access new avenues in nanotechnology.

(2) Dye-Sensitized and Bulk-Heterojunctions Solar Cells: TiO_2 Nanotube Arrays as a Base Material

As the abbreviation of dye-sensitized solar cell, DSC is a photovoltaic device with low economic cost by a photosensitized anode and hole transporting electrolyte. When the dye stays between the semiconductor and electrolyte, the separation of charge happens. The efficiency of DSC peaks at 11% via nanocrystalline TiO_2 films. There are two main factors restricting the promotion of photoconversion efficiency in such DSCs: the first one stems from slow percolation of electrons via the random polycrystalline network; the second one is based on the poor absorption of low energy photons by the available dyes. In this paper, we focus on the promotion of anodically grown utility and choose the TiO_2 nanotube arrays as the base electron transporting material by providing large surface areas with vectorial charge transport along the length of the nanotubes. Polymer-based solar cells have the advantage of lightweight, flexible photovoltaics and low industrial costs. The paper of Heeger et al. implied a peak percentage of 6.5 efficiency via tandem solar cells, with each layer processed from solution with the use of bulk heterojunction materials comprising semiconducting polymers and fullerene derivatives. On the basic of conjugated polymers, devices of inorganic–organic hybrid photovoltaic does good in combining the electron mobility of inorganic semiconductors. Aiming to offer intimate bulk heterojunctions for exciton splitting as well as unique path for the application of electron and hole transport, inorganic n-type nanocrystals are commonly dispersed in conjugated p-type polymer matrices. Anyway, in terms of such kind of heterojunction device, both organic and inorganic phases produce chaotic networks, which lacks a successive electronic photogenerated transport path. Thus in a fixed time period, isotropic host organic material transports both of the above mentioned charging carrier. Adding to the random charging carrier path, such issue

promotes the recombination possibility, which resulting to a decline of photoconversion efficiency in general. To handle these issues, academic studies suggest that the favorable heterojunction geometry of an inorganic-organic device should include a vertical array of highly crystallized nanostructures, such as nanotubes or nanorods, encased in a polymer film with size and spacing of the nanostructures controlled to be on the order of the exciton diffusion length. The theory of geometry offers an inspiration to separate the charging transport channels, severally. Correspondingly, efforts for the further development of TiO_2 nanopores and nanotubes, ZnO and SnO_2 nanorods, etc. Have been carried out to create films with ordered one-dimensional architectures. As a result, the fundamental material is selected as TiO_2 nanotube array, cautiously the under the applying principle of bulk heterojunction devices and the development of polymeric solar cells.

(3) Use of TiO_2 Nanotube Arrays for Biological Applications

Empirical methods in the area of biology and biophysics are treated as the cornerstone of protein immobilization on solid substrates. To distinguish the difference between protein–protein, protein–DNA, and protein–molecule interactions for many diagnostic and profiling use, immobilized proteins are operated as general instruments. And it is necessary for the supporting material to have the feature of positive surface, for the purposes of binding protein, keeping mechanical, thermal, and chemical stability. The sensitive detection of affinity-based interactions between complementary molecule pairs is typically allowed via electrical signals in bioelectrocatalytic systems. While a useful and convenient employment in biomedical diagnosis as well as environmental analysis is provided by amperometric biosensors. This section take the utility of co-immobilized TiO_2 nanotube arrays into consideration as a H_2O_2 and glucose detection platform. Because of the merit of high strength, biocompatibility and high level of hemocompatibility, Titanium and related alloys have been generally applied as implants. In most daily environment, the ability of Ti alloy biocompatibility produces steady and dense oxide layers. Researchers have reached an agreement that oxide surface with thick and steady TiO_2 is advanced for surface bioactivity. Spark anodization is widely

employed to enhance the biocompatibility of titanium and related alloys, with the process leading to the formation of a disordered oxide structure several hundred nanometers thick. On the opposite of this method,the electrochemical formation of highly ordered TiO_2 nanotube arrays offer a unique surface for biomedical implants that offers both biocompatibility as well as drug eluting properties. Overall, this section looks back into the real world utility of TiO_2 nanotube arrays in the promotion of apatite formation, cell activity, drug elution, and the application of TiO_2 nanotubular membranes for protein separation and drug delivery.

3.6. Conclusions for this chapter

In this chapter, we introduced TNTs, the highly-ordered TNTs were fabricated by anodization method, the morphology of TNTs was characterized by SEM. The electrochemical performances of the samples were examined by electrochemical workstation. Finally summarize the main points are:

1. The introduction of TNTs, and different fabrication methods of TNTs.
2. The TiO_2 nanotubes are fabricated by anodization method.
3. UV-vis spectroscopy analysis the absorption spectra of TiO_2 powder, pristine TNT arrays prepared at 60V/1h.
4. CV tests displays the CV curves of pristine 60V/6h, 60V/12h and 60V/16h TiO_2 nanotube arrays as a function of scan rates measured in a three-electrode configuration.
5. The application of highly ordered TNTs.

Chapter 4 Photon Absorption Enhancement of TiO_2 Nanotube Arrays Decorated with Aluminum Nanoparticles

(This section has been accepted by ECS Transaction, 2017, article in press)

Since more than ten years ago, the management and remediation of environment pollution have obtained great achievement due to optoelectronic applications, which is treated as a potential and meaningful method to overcome global energy shortage and remitting the pollution problems. Firstly, the scholars have paid attention to the development of visible light-active semiconductors with high optoelectronic efficiency. Specifically, composites on the basic of TiO_2 have aroused hot debates due to their advantage of chemical stability, lovely price, and environmental friendly. Whereas the only fly in the ointment stems from the fact that single TiO_2 has low optoelectronic sensitivity due to the fast recombination of photogenerated electrons and holes, narrow light-absorption range, and lack of effective reactive sites.

To cope with the questions, various strategies have been utilized to modify properties of TiO_2 nanomaterials, including gas phase process, metal and nonmetal decoration, dyes sensitization. In terms of metal decoration, the metallic nanoparticles with feature of random size and distribution contribute to high density of localized surface plasmon resonance (LSPR). And LSPR is defined as an effect that generates dramatic peaks in extinction spectra, as well as intensive increase of the local electromagnetic fields surrounding the nanoparticles. Furthermore, TiO_2 nanotube arrays decorated with metal nanoparticles shows much advantages for achieving high performance, such as plasmon-enhanced solar desalination, plasmon-photocurrent enhancement, and plasmon-enhanced catalytic reactions.

4.1. Introduction of aluminum nanoparticles for plasmonics

The abovementioned metals inherently have shortcomings in blocking the plasmonic devices blossom of the EM spectrum, especially towards blue and ultraviolet (UV) parts. To be specific, gold shows weak plasmonic resonances at wavelengths shorter than 520 nm because of the feature of inter-band transitions. Even though nanostructures by silver material represents LSPRs for less than 350 nm, it is not able to come across intensive oxidation and misses plasmonic properties as time passing by. Focusing on these shortcomings, aluminium (or Al) plasmonics have been developed. Because of aluminum's original properties, for instance, it owns high plasma energy of 15.6 ev, it does good in supporting surface plasmons in the visible-light region. Compared to noble metals like gold and silver, aluminium is economical-friendly and easily-accessible on our planet of earth. Such advantage is of vital importance to industrial applications to achieve huge economic interest. Thus metal of aluminium gives path to plasmonic engineering of optical properties, which has the power to open the global optoelectronic market. Broadly speaking, plasmonics by metal of aluminium remains popular in industrial applications, for instance, in the field of metal enhanced fluorescence, label-free biosensing applications, non-linear plasmonics, light harvesting devices, photodetection, photocatalysis or high data density storage.

In this work, we focus on loading aluminum nanoparticles product on TNTs by a facile decoration technique, expecting to enhance visible light absorption as well as their photocurrent. Amount of the aluminum nanoparticles on crystalline anatase nanotubes were tuned by magnetron sputtering deposition technique with different thickness of aluminum nanoparticles. Microstructure and photon spectrum absorption properties of the decorated nanotube composites examined by physical techniques such as scanning electron microscopy (SEM) and UV-Visible absorption spectroscopy are reported. Meanwhile, I-V characteristics and transient photocurrent responses of the decorated TNTs composites are characterized by photoelectric measurement method,

further revealing intrinsic characteristics of electron generation, separation, and transportation in TiO_2-Al systems.

4.2. Experiment

4.2.1 Materials and lab equipment

This chapter focuses on TiO_2 nanotube arrays decorated with aluminum nanoparticles and how the decorated composites affect the electrochemical characteristics of TiO_2 electrode material. The fabrication of the highly-ordered TNTs is the same as described in chapter 3, lab equipment is the same as described in chapter 2.

4.2.2. The fabrication of highly ordered TNTs

The fabrication of highly ordered TNTs is the same procedures as described in chapter 3.

4.2.3. The fabrication of aluminum nanoparticles

4.2.3.1. The fabrication of aluminum nanoparticles on the glass substrates.

The step is that Aluminum nanoparticles were prepared by a radio frequency (RF) reactive magnetron sputtering system (Sputter AJA 4050) using aluminum (99.9% purity) target. The glass substrate was clean in ethyl alcohol solution. The chamber was at a base pressure(4.2mTorr), power (120 W), gas (10 scan), the beginning of deposition rate (0.28 Å/S), stable deposition rate (0.4 Å/S). By adjusting the sputtering time, Al thickness ranging from zero to twenty nm on the glass substrates. The empirical evidence of different nanoparticles Al on square glass for 22mm multiply by 22mm is shown in Figure 4.2.

4.2.3.2. The fabrication of aluminum nanoparticles on the TiO_2 substrates.

The TiO_2 nanotube substrate was prepared in chemical method before deposition. The dimension of nanoparticles Al have been calibrated on TiO_2 substrates with thickness from 0 to 20 nm, the deposition method is the same as above. Schematic process for fabricating aluminum nanoparticles of TiO_2 nanotubes is shown in the figure 4.1. The dimension of nanoparticles Al have been calibrated on TiO_2 with thickness from 0 to 20 nm, which can be controlled by the sputtering time, photograph of various nanoparticles Al on TiO_2 (10mm×20mm) is shown in the figure 4.2.

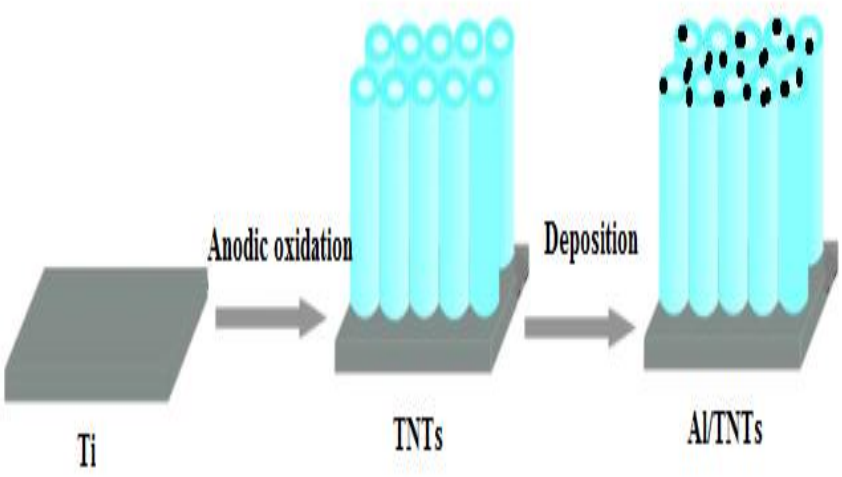

Fig.4.1 Schematic process for fabricating aluminum nanoparticles of TiO_2 nanotubes

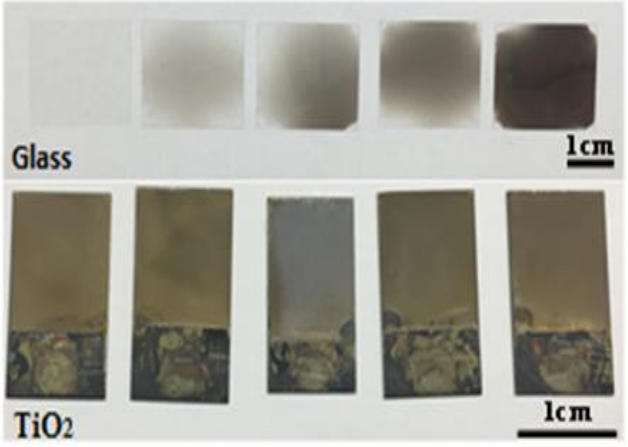

Fig. 4.2 Photograph of various nanoparticles Al on glass and TiO_2 sputtered with different thickness. From left to right, 0 nm,5 nm, 10nm,15nm, 20 nm.

4.3. Characterization

4.3.1. Morphologies

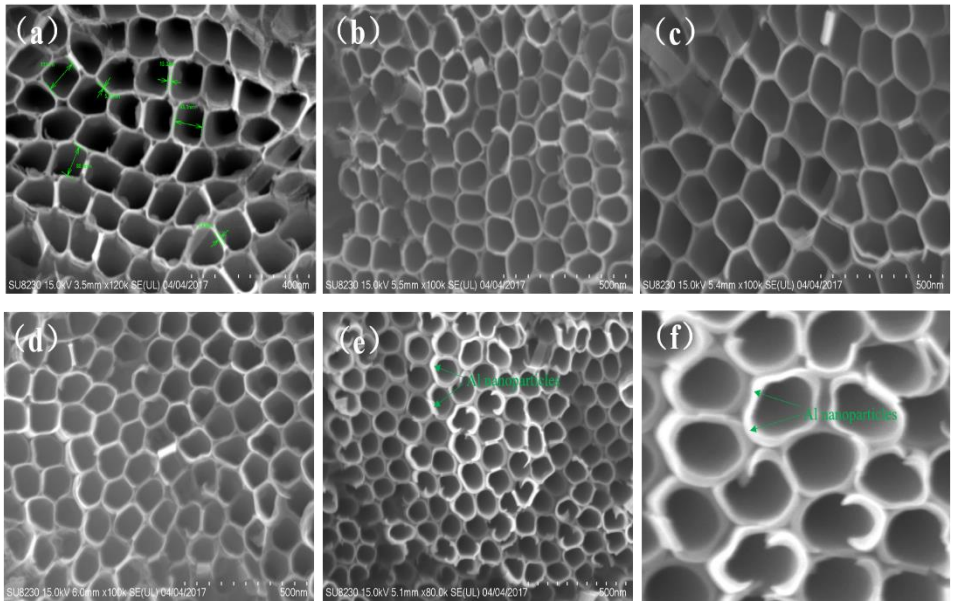

Fig. 4.3 (a) SEM images of TNTs, (b) 5 nm Al-TNT, (c) 10 nm Al-TNT, (d) 15 nm Al-TNT, (e) 20 nm Al-TNT, (f) Magnification SEM image of TNTs with Al nanoparticles.

Fig. 4.3 shows the top-view SEM images of TNT, 5 nm Al-TNT, 10 nm Al -TNT, and 15 nm Al -TNT, 20 nm Al-TNT. As-prepared samples were clearly observed a periodically porous structure with an average diameter of ~90 nm and a wall thickness of ~9 nm. The Al/TiO_2 NTs have well-ordered and uniformly arranged tubular structure. Al NPs (5 – 20 nm) were successfully prepared which were highly and uniformly dispersed on the surface of TiO_2 NTs.

Figure 4.4 shows top-view SEM image of well-aligned crystalline of Al/TiO_2 NTs arrays and the composition of Al/TiO_2 NTs. Because Al NPs (5-20 nm) has a uniform arrangement and good tubular structure. It highly uniform distribution on the surface of TiO_2 nanotubes. By EDS test, SEM chamber chimeric was used to determine the combination of the content of titanium dioxide/TiO_2 NTS. EDS spectrum showed that the compose of Ti, O and Al. The percentage of Al in composite materials increase with the increase of the thickness of Al NPs. The strong interaction between TiO_2 and Al NPs is due to Al NPs evenly dispersed, and improves the charge transfer and separation,

during this experiment also found that due to reduce the surface reflection and increase internal light scattering. As well as the host stand close packing of aluminum NPs, unique nanometer TiO_2 can further improve the total absorption properties of porous structure.

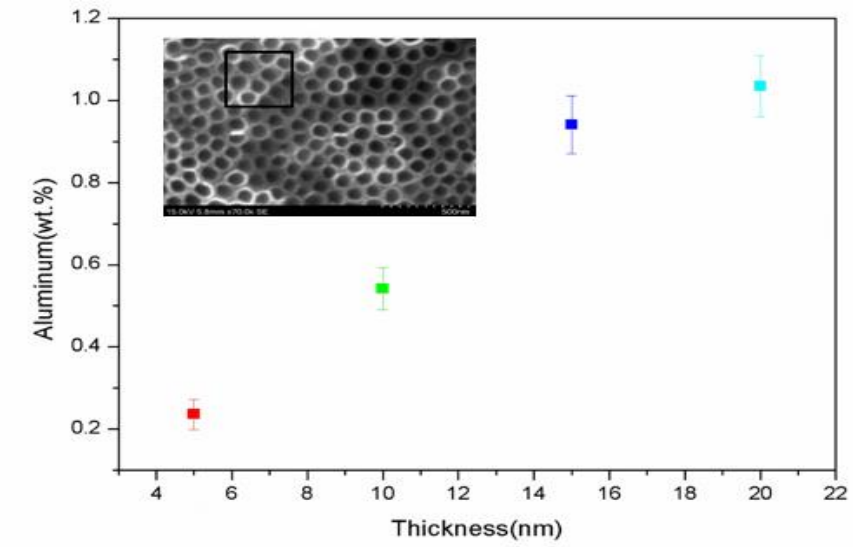

Fig. 4.4 Top-view SEM image of well-aligned crystalline of Al/TiO_2 NTs arrays and the composition of Al/TiO_2 NTs.

Plasma structure can make a very effective broadband solar absorption, mainly through the following mechanisms: (1) aluminum nanoparticles not only provides additional encapsulation protecting natural oxidation stability, also changed the environment for the effective dielectric constant and thus to further broaden the range of visible light absorption within the bandwidth. (2) Aluminum self-assembled nanoparticles are often greeted on TiO_2 nano hole wall (in the cross section of the SEM images shows), strong plasma hybrid effect and high density of LSP resonance excitation.

4.3.2. UV-vis spectroscopy analysis

4.3.2.1. Absorption spectra of nanoparticles Al on the glass substrates

Figure 4.5 shows absorption spectra (220 - 850 nm) of pristine glass, 5nm Al/glass, 10nm Al/glass,15nm Al/glass, 20nm Al/glass. The pristine glass has weak absorption of visible light at the wavelength above 400 nm. The absorptive spectra of Al/glass have

been enhanced at the visible light region from 400 nm to 800 nm after decorating with the thickness of Al NPs. Therefore, Al nanoparticles are remarkable visible light harvesting material for furnishing the glasses. The 20 nm Al/glass sample exhibited a highest absorption value in the visible light region. The enhanced visible light absorption value could be ascribed to the increased localized surface plasmon resonance (LSPR) of Al nanoparticle.

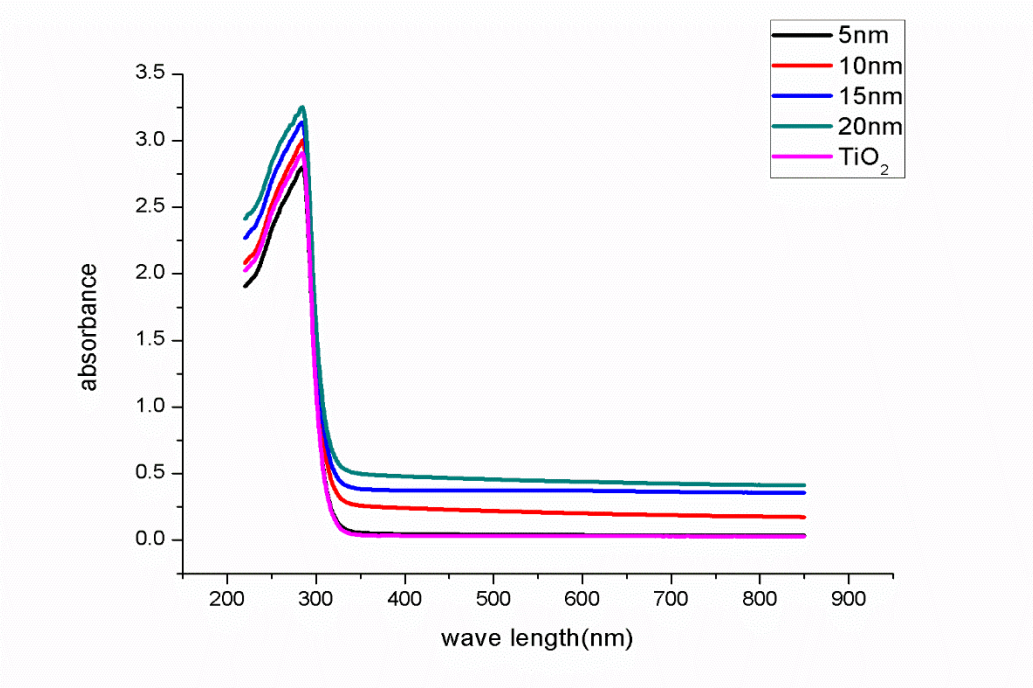

Fig. 4.5 UV-vis absorption spectra of pristine glass, 5nm Al/glass, 10nm Al/glass,15nm Al/glass, 20nm Al/glass.

4.3.2.2. Absorption spectra of nanoparticles Al on the TiO_2 substrates

Absorption spectra (400 ~850 nm) confirmed that with the increase of the thickness of the Al NPs, the absorption peak intensity increases, compared with pure TiO_2. 10 nm Al/NTS NTS samples showed a wide range of absorption peak center near 550 nm visible light area. Enhanced visible light absorption peaks can be attributed to the increase of local surface plasmon resonance (LSPR) nano aluminum. These results indicate that the optical response of the titanium dioxide can be easily extended to the help of the visible light region, Al NPs, sees Figure 4.6.

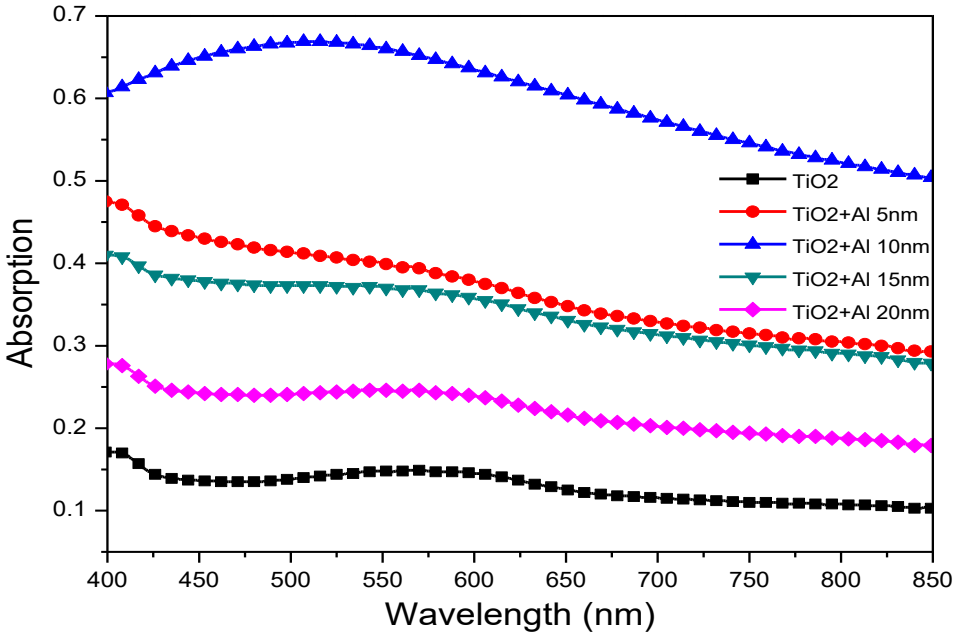

Fig. 4.6 UV-vis absorption spectra of pristine TNTs, TNTs/5nm Al, TNTs/10nm Al, TNTs/15nm Al, TNTs/20nm Al

4.3.2.3 Photocurrent characteristics of nanoparticles Al on the TiO_2 substrates

In Figure 4.7, it shows I-V characteristics of pristine TNTs, 5 nm Al/TNTs, 10 nm Al/TNTs, 15 nm Al/TNTs, and 20 nm Al/TNTs in under white light illumination. In Figure 4.7, with Al nanoparticles (5 – 20 nm) incorporation, the photocurrents were distinctively enhanced in all samples. Strong similarity can be observed between the UV–vis spectra of the corresponding Al nanoparticles incorporated in them. It is obvious that the maximum photocurrent of 0.07 mA is obtained by 10 nm Al/TiO_2 NTs sample at bias potential of 0.5 V, while only 0.34 mA for pure TiO_2 NTs is observed. This result indicates that the photocurrent enhancements are plasmon-induced and the separation rate of photo-generated holes and electrons increased. The saturated photocurrent of the 10nm Al/TiO_2 NTs was 1.9 times higher than that of the bare TiO_2 NTs at 0.7 V.

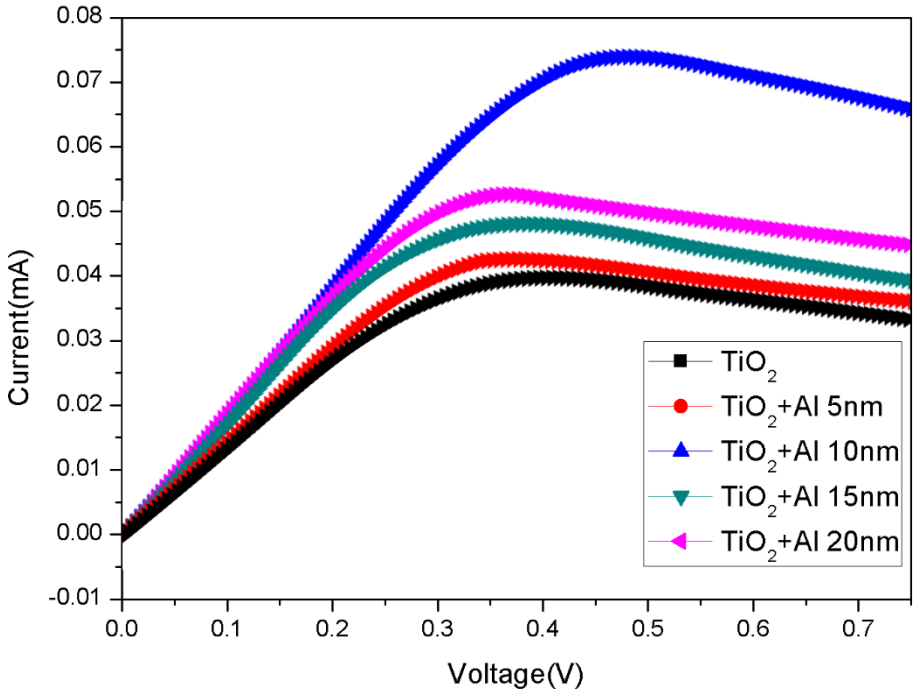

Fig. 4.7 I-V characteristics of pristine TNTs, 5nm Al/TNTs, 10nm Al/TNTs, 15nm Al/TNTs, and 20nm Al/TNTs in under white light illumination.

4.3.3. Photocurrent response of nanoparticles Al on the TiO_2 substrates

Under the condition of light, through ring opening light many times call charge separation photocurrent response measurement. Measured at 1 V, and said the reproducibility and stability of the optical response. When the light source is opened, the photocurrent transient rise, once the lighting was shut down, immediately return to its original value. Repeatability and stability of the optical response can be attributed to a coherent system interface, allowing efficient electron transfer from aluminium to TiO_2 nanotube arrays. Compared with current response in pristine TNTs, the photocurrents in TNTs/5 nm Al, TNTs/10 nm Al, TNTs/15 nm Al, TNTs/20 nm Al are increased up to several times under white light illumination with bias potential, the photocurrent of TNTs/10 nm Al is much higher than the ones which decorated with TNTs in figure 4.8. High sensitive current could be due to two reasons: the existence of the plasma 10 nm aluminum nanoparticles, greatly expanded the TiO_2 - NTs response to the visible light

region. In addition, the low combination of photogenerated electrons and holes can facilitate the separation and transfer of photogenerated electrons.

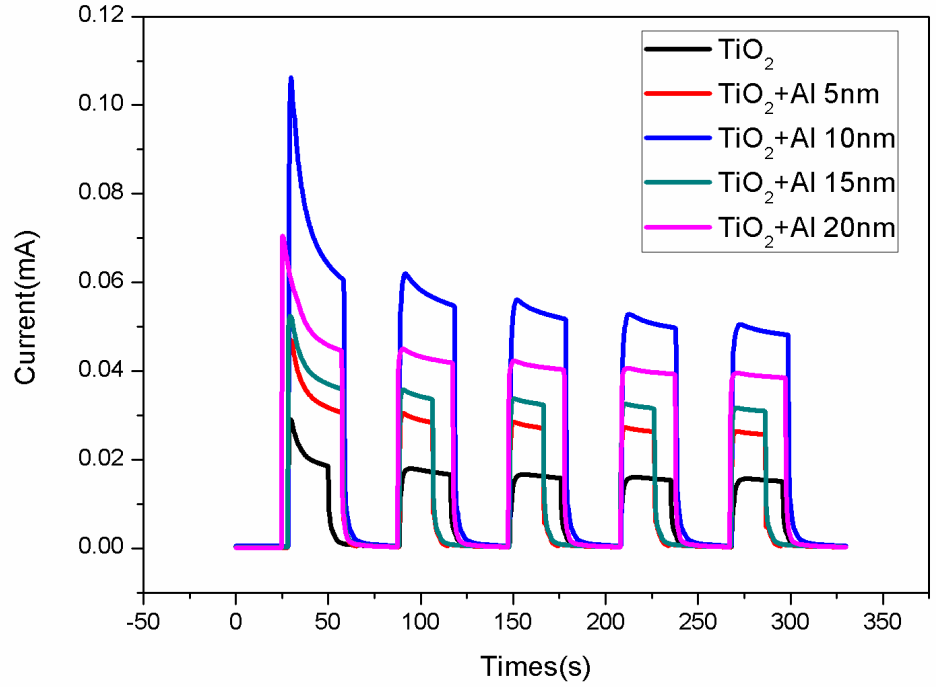

Fig. 4.8. Photocurrent response of pristine TNTs, 5nm Al/TNTs, 10nm Al/TNTs, 15nm Al/TNTs, and 20nm Al/TNTs under white light illumination

4.3.4. EIS analysis.

As the electrodes and the electrolyte on the electrode for powerful work to charge transfer, effective detection of charge carrier separation efficiency. We usually use a large circular radius represents a larger charge transfer resistance, in the process, reduce the separation efficiency of the light hole electron pair. As shown in figure 4.9, Al/TiO_2 NTS impedance arc radius are much smaller than the original TiO_2. This shows that the Al/TiO_2 NTS show greater separation efficiency of light produced by the electron - hole on the charge transfer and faster than original TiO_2 NTS in the solid-liquid interface.

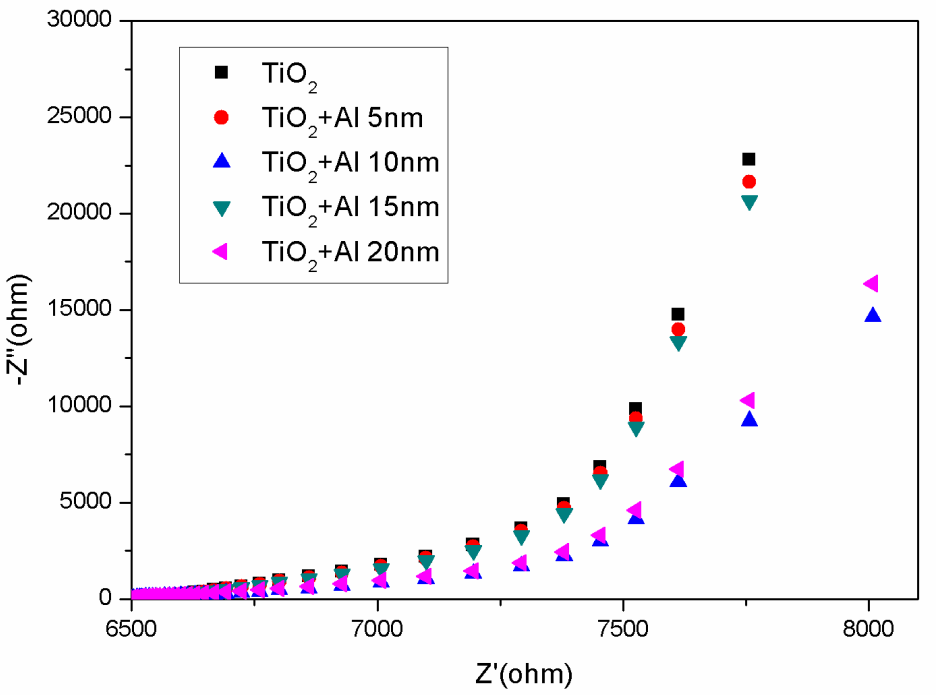

Fig. 4.9. EIS responses of pristine TiO_2 NTs, 5 nm Al/TNTs, 10 nm Al/TNTs, 15 nm Al/TNTs, and 20 nm Al/TNTs under white light illumination

4.4 Conclusions

This chapter realizes well-aligned TiO_2 nanotubes (TNTs) decorated with aluminum nanoparticles have been fabricated by electrochemical anodization and subsequently magnetron sputtering technique. The morphology of the decorated TNTs was characterized using SEM, EDS analysis and employed to determine the crystal structure, UV-vis light absorbance spectra were recorded by a UV-vis spectrophotometer. The electrochemical characteristics of decorated TNT nanotubes were studied by CV, EIS measurements. Finally summarize the main points of electrochemical aluminum nanoparticles decorated of TNT nanotubes are:

1. After electrochemical loading, the color of the 10 nm AL/TNTs changes significantly to black. But other TNT arrays are still compacted, highly ordered, cylindrical nanotubes.

2. For the 10 nm Al/TiO_2 NTs sample, the absorption spectra is larger than that of the pristine TNTs, 5 nm Al/TiO_2 NTs sample, 15 nm Al/TiO_2 NTs sample, 20 nm Al/TiO_2 NTs sample. This means that the 10 nm Al/TiO_2 nanotubes samples showed a wide

range of absorption peak near 550 nm, enhanced visible light absorption peaks can be attributed to the increase of local surface plasmon resonance (LSPR).

3. We compare the photocurrent of decorated TNTs with thickness of 5 nm, 10 nm, 15 nm, 20 nm. So the increasing thickness of the 10 nm Al nanoparticles creates a significantly higher photocurrent value, which leads to the enhancement of the photocurrent responses.

4. We compare with current response in pristine TNTs, the photocurrents in TNTs/5 nm Al, TNTs/10 nm Al, TNTs/15 nm Al, TNTs/20 nm Al are increased up to several times under white light illumination with bias potential, the photocurrent of TNTs/10 nm Al is much higher than the ones which decorated with TNTs.

5. The impedance of Al/TiO_2 NTs decreases with the increasing the thickness of Al NPs, the impedance of the 10 nm Al/TiO_2 NTs is obviously smaller than that of the pristine TiO_2 NTs.

Chapter 5 Conclusions

5.1. The main conclusions of this thesis

In this thesis, the applications of TiO_2 nanotube arrays are studied. The fabrication of TNTs is realized by anodization. One novel approach to improve the electrochemical characteristics is conducted: firstly, anodization method to prepare TNT nanotubes; secondly, the synthesis of plasmonic Al nanoparticles decorated with TiO_2 NTAs by a sputtering system, which is called RF (radio freuency). The measurements of morphology, crystal structure and electrochemical characteristics of TNTs are recorded. The measurements data approved that this approach can enhance the electrochemical characteristics of TNT electrodes significantly.

In summary, the electrochemical characteristics of decorated TNTs have demonstrated that the 10 nm Al nanoparticles decorated TNT arrays show ideal behavior and enhance the electrochemical characteristics of TiO_2. It is also found that plasmonic Al NPs can significantly enhance the absorption intensity of TiO_2 NTs in the visible region. The 10 nm nanoparticles Al decorated with TiO_2 NTs showed significantly higher photocurrent value than pristine TiO_2 NTs due to better charge separation under white light illumination. Metallic nanoparticles Al decorated TiO_2 NTs was prepared by using an electrochemical anodization procedure and a magnetron sputtering technique. Al nanoparticles are the main absorption carriers, because Al nanoparticles are closely packed in random distributions, the LSPR of each Al nanoparticle will overlap and hybridize, leading to multiple overlapping plasmonic modes that give rise to broadband absorption. The high porosity porous template provides a strong reflection and scattering, optical path length was significantly increased. The synergy effect between nanotubular structures of TiO_2 and uniformly dispersed 10 nm Al nanoparticles, facilitated the Al plasmon-induced charge separation and transfer. It is expected that such Al/TiO_2 NTs electrode could be promisingly employed for various environmental pollutants utilizing solar energy.

5.2. The improvement of this thesis

In this work, a combined contribution from the plasmonic effect and long nanotube arrays are applied for achieving electrochemical characteristics of Al/TNTs. For better practical applications, we avoid either high conditions or expensive equipment to realize a facile technique with high efficiency. The synergy effect is realized by electrochemical loading processes which are simple and fast. As a key parameter, the plasmonic effect of decorated TiO_2 nanotubes can also be affected by the thickness, we fabricated Al/TNTs with different thickness. The experimental results indicate the electrochemical properties of decorated TNTs improve significantly, and with specific thickness, the electrochemical properties will show substantial enhancement which are fairly high in comparison with the previous reports.

5.3. Future work

In this thesis, one approach to improve the electrochemical characteristics of TNTs is conducted, except for one approach, we can develop more ways to improve the electrochemical properties of TNTs:

1. For the electrochemical loading, the main process is to deposit the Al nanoparticles on the TNTs. We can also try to add hybrid metal nanoparticles to improve the electrochemical properties of TNTs. Then study the electrochemical characteristics of decorated TNTs.
2. Instead of loading Al nanoparticles on the TiO_2 tubes, we can try to control the diameter of Al nanoparticles which can also results in the increasing of electrochemical properties.
3. The fabrication of TNTs is realized by anodization in this thesis; we can try other methods of fabrication of TNTs, and then study the results of loading.

Bibliography

[1] Z. Endut, M. Hamdi, W.J. Basirun, Surf. Coat. Tech, 215, 75 (2013).

[2] K. Hashimoto, H. Irie, A. Fujishima. J. Appl. Phys., 44, 8269 (2005).

[3] L. Wang, L. Jia, Q. Li, Mater. Lett, 123, 83 (2014).

[4] L. Jeurgens, W. Sloof, F. Tichelaar, E. Mittemeijer, Phys. Rev.62, 4707 (2000).

[5] S. Qian, C. Wang, W. Liu, Y. Zhu, W. Yao, X. Lu, J. Mater. Chem., 21, 4945 (2011).

[6] S. Linic, U. Aslam, C. Boerigter, M. Morabito, Nature Mater. 14, 567 (2015).

[7] M.W. Knight et al. ACS Nano 8, 834 (2014).

[8] D. Wang, J. Qian, F. Cai, S. He, S. Han, Y. Mu, Nanotechnology, 23, 245701 (2012).

[9] E. Prodan, C. Radloff, N. J. Halas, P. Nordlander, Science, 302, 419 (2003).

[10] J. Qiao, Q. Wang, Y. Xiao, J. Appl. Electrochem., 44, 1007 (2014).

[11] Andrew B. Ultracapacitors: Why, how and where is the technology [J]. Journal of Power Sources, 2001, 91:37-50.

[12] S. Chen, W. Liu, Mater. Chem. Phy., 98, 183 (2006).

[13] Conway B E. Electrochemical supercapacitor [J]. Scientific Fundamentals and Technological Applications, Kluwer Academic/Plenum Publishers, New York, 1999.

[14] Zhang Z A, Deng M G, Hu Y D, et al. Features and application of electrochemical capacitors [J]. Electronic Component and Materials, 2003, 22(11): 2-5.

[15] http://batteryuniversity.com/learn/article/whats_the_role_of_the_supercapacitor.

[16] http://www.azonano.com/article.aspx?ArticleID=3044

[17] A. Matsuda, S. Sreekantan, W. Krengvirat, Opt. Mater. Express, 5, 712 (2015).

[18] B. J. Morgan, G. W. Watson, J. Phys. Chem. C, 114, 2321 (2010).

[19] A. Fujishima, K. Honda, *Nature*, 238, 37 (1972).

[20] Tetraethylammonium tetrafluoroborate - Compound Summary Pub Chem 2724277.

[21] X. W. Zhang, M. H. Zhou, L. C. Lei, *Carbon*, 43, 1700 (2005).

[22] Conway B E. Electrochemical supercapacitor [J]. Scientific Fundamentals and Technological Applications, Kluwer Academic/Plenum Publishers, New York, 1999.

[23] http://www.murata.com/en-sg/products/capacitor/edlc/techguide/principle.

[24] K. Hashimoto, H. Irie, A. Fujishima, *Jpn. J. Appl. Phys.*, **44**, 8269 (2005).

[25] G. Q. Ji, Z. Q. Liu, D. B. Guan, Y. T. Yang, *Appl. Surf. Sci.*, **282**, 695 (2013).

[26] J. Moa, Y. Zhang, Q. Xu, J.J. Lamson, R. Zhao, *Atmos. Environ.*, **43**, 2229 (2009).

[27] Ma R Z, Wei B Q, Xu C L, et al. Supercapacitors based on carbon-nanotubes [J]. China Science, 2000, 30(2): 112~116.

[28] Pitcher G. If the cap fits [J]. Portable Products Special Report, New Electronics, 2006: 25-26.

[29] Y. Li, L. Wei, X. Chen, R. Zhang, X. Sui, Y. Chen, L. Mei, *Nanoscale Res Lett*., **8**, 1 (2013).

[30] J. Lim, W. K. Bae, J. Kwak, S. Lee, C. Lee, K. Char, *Opt. Mater. Express*, **2**, 594 (2012).

[31] Cap-XX, Supercapacitors for Automotive & Other Vehicle Applications, March 2012.

[32] "The electrical double layer". 2011. Retrieved 20 January 2014.

[33] Raymundo-Pinero E, Kierzek K, Machnikowski J, et al. Relationship between the nanoporous texture of activated carbons and their capacitance properties in different electrolytes [J]. Carbon, 2006, 44 (12): 2498- 2507.

[34] S. Qian, C. Wang, W. Liu, Y. Zhu, W. Yao, X. Lu, *J. Mater. Chem.*, **21**, 4945 (2011).

[35] J. Luo, L. Ma, T. He, C. F. Ng, S. Wang, H. Sun, H. J. Fan, *J. Phys. Chem. C*, **116**, 11956 (2012).

[36] Xu B, Wu F, Chen R, et al. Mesoporous activated carbon fiber as electrode material for high-performance electrochemical double layer capacitors with ionic liquid electrolyte [J]. Journal of Power Sources, 2010, 195 (7): 2118-2124.

[37] Fang B, Binder L. A modified activated carbon aerogel for high-energy storage in electric double layer capacitors [J]. Journal of power sources, 2006, 163 (1):616-622.

[39] Ahmadpour A, Do D D, The preparation of activated carbon from macadamia nutshell by chemical activation [J]. Carbon, 1997, 35(12): 1723-1732.

[40] M. Wang, L. Sun, Z. Lin, J. Cai, K. Xie, C. Lin, *Energ. Environ. SCI.*, **6**, 1211 (2013).

[41] I. Moreels, K. Lambert, D. Smeets, D. De Muynck, T. Nollet, J. C. Martins, Z. Hens, *ACS nano*, **3**, 3023 (2009).

[42] Iijima S. Helical microtubules of graphitic carbon [J]. Nature, 1991, 354(6348): 56-58.

[43] Chen J H, Li W Z, Wang D Z, et al. Electrochemical characterization of carbon nanotubes as electrode in electrochemical double-layer capacitors [J]. Carbon, 2002, 40(8): 1193-1197.

[44] Pekala R W. Organic aerogels from the polycondensation of resorcinol with formaldehyde [J]. Journal of Materials Science, 1989, 24(9): 3221-3227.

[45] D. Segets, J. M. Lucas, R. N. Klupp Taylor, M. Scheele, H. Zheng, A. P. Alivisatos, W. Peukert, *ACS Nano*, **6**, 9021(2012).

[46] J. Qiao, Q. Wang, Y Xiao, *J. Appl. Electrochem.*, **44**, 1007 (2014).

[47] Zheng J P, Cygan P J, Jow T R. Hydrous ruthenium oxide as an electrode material for electrochemical capacitors [J]. Journal of the Electrochemical Society, 1995, 142(8): 2699-2703.

[48] Y. Dong, J. Wen, F. Pang, Y. Luo, G. D. Peng, Z. Chen, T. Wang, *Opt. Mater. Express*, **5**, 712 (2015).

[49] L. Etgar, J. Park, C. Barolo, M. K. Nazeeruddin, G. Viscardi, M. Graetzel, *ACS Appl. Mater. Inter.*, **3**, 3264 (2011).

[50] Zhang F, Zhou Y, Li H. Nanocrystalline NiO as an electrode material for electrochemical capacitor [J]. Materials Chemistry and Physics, 2004, 83(2): 260-264.

[51] M. M., Tavakoli, A. Simchi, H. Aashuri, *Mater. Chem. Phys.*, **156**, 163 (2015).

[52] P. Simon, L. Bahrig, I. A. Baburin, P. Formanek, F. Röder, J. Sickmann, E. Rosseeva, *Adv. Mater.*, **26**, 3042 (2014).

[53] Rudge A, Davey J, Raistrick I, et al. Conducting polymers as active materials in electrochemical capacitors [J]. Journal of Power Sources, 1994, 47(1): 89-107.

[54] Nanomaterials. European Commission. Last updated 18 October 2011

[55] Austin R H, Lim S. The Sackler Colloquium on promises and perils in nanotechnology for medicine [J]. Proceedings of the National Academy of Sciences, 2008, 105(45): 17217-17221.

[56] Fujishima A. Electrochemical photolysis of water at a semiconductor electrode [J]. nature, 1972, 238: 37-38.

[57] Lee S, Jeon C, Park Y. Fabrication of TiO2 tubules by template synthesis and hydrolysis with water vapor [J]. Chemistry of materials, 2004, 16(22): 4292-4295.

[58] Lee J H, Leu I C, Hsu M C, et al. Fabrication of aligned TiO_2 one-dimensional nanostructured arrays using a one-step templating solution approach [J]. The Journal of Physical Chemistry B, 2005, 109(27): 13056-13059.

[59] Jung J H, Kobayashi H, van Bommel K J C, et al. Creation of novel helical ribbon and double-layered nanotube TiO_2 structures using an organogel template [J]. Chemistry of materials, 2002, 14(4): 1445-1447.

[59] Miyauchi M, Tokudome H, Toda Y, et al. Electron field emission from TiO2 nanotube arrays synthesized by hydrothermal reaction [J]. Applied physics letters, 2006, 89(4): 3114.

[60] Gong D, Grimes C A, Varghese O K, et al. Titanium oxide nanotube arrays prepared by anodic oxidation [J]. Journal of Materials Research, 2001, 16(12): 3331-3334.

[61] Paulose M, Shankar K, Varghese O K, et al. Application of highly-ordered TiO2 nanotube-arrays in heterojunction dye-sensitized solar cells [J]. Journal of Physics D: Applied Physics, 2006, 39(12): 2498.

[62] Tan L K, Chong M A S, Gao H. Free-standing porous anodic alumina templates for atomic layer deposition of highly ordered TiO2 nanotube arrays on various substrates [J]. The Journal of Physical Chemistry C, 2008, 112(1): 69-73.

[63] http://www.scs.illinois.edu/murphy/Ran/research/templatesynthesis.html

[64] Yu J, Yu H. Facile synthesis and characterization of novel nanocomposites of titanate nanotubes and rutile nanocrystals [J]. Materials chemistry and physics, 2006, 100(2): 507-512.

[65] Zhang Q, Gao L, Sun J, et al. Preparation of Long TiO2 Nanotubes from Ultrafine Rutile Nanocrystals [J]. Chemistry Letters, 2002 (2): 226-227.

[66] Wang W, Varghese O K, Paulose M, et al. A study on the growth and structure of titania nanotubes [J]. Journal of materials research, 2004, 19(02): 417-422.

[67] D.F. Zhang, Russ. J. Phys. Chem. A 86 (2012) 498–503.

[68] Tian Z R, Voigt J A, Liu J, et al. Large oriented arrays and continuous films of TiO2-based nanotubes [J]. Journal of the American Chemical Society, 2003, 125(41): 12384-12385.

[69] Vuong D D, Tram D T N, Pho P Q, et al. Hydrothermal synthesis and photocatalytic properties of TiO_2 nanotubes[M]//Physics and Engineering of New Materials. Springer Berlin Heidelberg, 2009: 95-101.

[70] Macak J M, Tsuchiya H, Ghicov A, et al. TiO_2 nanotubes: self-organized electrochemical formation, properties and applications [J]. Current Opinion in Solid State and Materials Science, 2007, 11(1): 3-18.

[71] Zwilling V, Aucouturier M, Darque-Ceretti E. Anodic oxidation of titanium and TA6V alloy in chromic media. An electrochemical approach [J]. Electrochimica Acta, 1999, 45(6): 921-929.

[72] N. Kruse, S. Chenakin, Appl. Catal. A: Gen. 391 (2011) 367–376.

[73] Gong D, Grimes C A, Varghese O K, et al. Titanium oxide nanotube arrays prepared by anodic oxidation [J]. Journal of Materials Research, 2001, 16(12): 3331-3334.

[74] Varghese O K, Gong D, Paulose M, et al. Crystallization and high-temperature structural stability of titanium oxide nanotube arrays [J]. Journal of Materials Research, 2003, 18(1): 156-165.

[75] Ruan C, Paulose M, Varghese O K, et al. Fabrication of highly ordered TiO2 nanotube arrays using an organic electrolyte [J]. The Journal of Physical Chemistry B, 2005, 109(33): 15754-15759.

[76] Macak J M, Tsuchiya H, Taveira L, et al. Smooth anodic TiO_2 nanotubes [J]. Angewandte Chemie International Edition, 2005, 44(45): 7463-7465.

[77] Prakasam H E, Shankar K, Paulose M, et al. A new benchmark for TiO_2 nanotube array growth by anodization [J]. The Journal of Physical Chemistry C, 2007, 111(20): 7235-7241.

[78] S.K. Ghosh, T. Pal,Chem. Rev. 107 (2007) 4797–4862.

[79] Richter C, Wu Z, Panaitescu E, et al. Ultra‐High‐Aspect‐Ratio Titania Nanotubes [J]. Advanced Materials, 2007, 19(7): 946-948.

[80] Macák J M, Tsuchiya H, Schmuki P. High‐Aspect‐Ratio TiO2 Nanotubes by Anodization of Titanium [J]. Angewandte Chemie International Edition, 2005, 44(14): 2100-2102.

[81] Salari M, Aboutalebi S H, Konstantinov K, et al. A highly ordered titania nanotube array as a supercapacitor electrode [J]. Physical Chemistry Chemical Physics, 2011, 13(11): 5038-5041.

[82] Chen X, Mao S S. Titanium dioxide nanomaterials: synthesis, properties, modifications, and applications [J]. Chemical reviews, 2007, 107(7): 2891-2959.

[83] Wu H, Xu C, Xu J, et al. Enhanced supercapacitance in anodic TiO_2 nanotube films by hydrogen plasma treatment [J]. Nanotechnology, 2013, 24(45): 455401.

[84] Paulose M, Shankar K, Yoriya S, et al. Anodic growth of highly ordered TiO_2 nanotube arrays to 134 μm in length [J]. The Journal of Physical Chemistry B, 2006, 110(33): 16179-16184.

[85] Gong J, Pu W, Yang C, et al. A simple electrochemical oxidation method to prepare highly ordered Cr-doped titania nanotube arrays with promoted photoelectrochemical property [J]. Electrochimica Acta, 2012, 68: 178-183.

[86] Shankar K, Tep K C, Mor G K, et al. An electrochemical strategy to incorporate nitrogen in nanostructured TiO2 thin films: modification of bandgap and photoelectrochemical properties [J]. Journal of Physics D: Applied Physics, 2006, 39(11): 2361.

[87] Liu G, Wang K, Hoivik N, et al. Progress on free-standing and flow-through TiO2 nanotube membranes [J]. Solar Energy Materials and Solar Cells, 2012, 98: 24-38.

[88] Liu G, Hoivik N, Wang K, et al. Reducing solvent evaporation rates for the detachment of anodic TiO_2 nanotubular membranes[C]//MRS Proceedings. Cambridge University Press, 2012, 1442: mrss12-1442-q06-02.

[89] Roy P, Berger S, Schmuki P. TiO_2 nanotubes: synthesis and applications [J]. Angewandte Chemie International Edition, 2011, 50(13): 2904-2939.

[90] Sreekantan S, Hazan R, Lockman Z. Photoactivity of anatase–rutile TiO_2 nanotubes formed by anodization method [J]. Thin Solid Films, 2009, 518(1): 16-21.

[91] M. Murdoch, G.I.N. Waterhouse, M.A. Nadeem, J.B. Metson, M.A. Keane, R.F.Howe, J. Llorca, H. Idriss, Nat. Chem. 3 (2011) 489–492.

[92] G.S. Li, B. Jiang, S.N. Xiao, Z.C. Lian, D.Q. Zhang, J.C. Yu, H.X. Li, Environ. Sci. 16 (2014) 1975–1980.

[93] X.L. Liu, Y.H. Han, G.Y. Li, H.M. Zhang, H.J. Zhao, RSC Adv. 3 (2013) 20824–20828.

[94] Macak J M, Gong B G, Hueppe M, et al. Filling of TiO_2 Nanotubes by Self-Doping and Electrodeposition [J]. Advanced Materials, 2007, 19(19): 3027-3031.

[95] Sousa S R, Moradas-Ferreira P, Saramago B, et al. Human serum albumin adsorption on TiO_2 from single protein solutions and from plasma [J]. Langmuir, 2004, 20(22): 9745-9754.

[96] Xing M, Fang W, Nasir M, et al. Self-doped Ti3+-enhanced TiO_2 nanoparticles with a high-performance photocatalysis [J]. Journal of Catalysis, 2013, 297: 236-243.

[97] Zhou H, Zhang Y. Electrochemically self-doped TiO_2 nanotube arrays for supercapacitors [J]. The Journal of Physical Chemistry C, 2014, 118(11): 5626-5636.

[98] Y.H. Zhang, Y.N. Yang, P. Xiao, X.N. Zhang, L. Lu, L. Li, Mater. Lett. 63 (2009)2429–2431.

[99] Chen W P, Wang Y, Chan H L W. Hydrogen: a metastable donor in TiO_2 single crystals [J]. Applied physics letters, 2008, 92: 1-3.

[100] Wang K, Liu G, Hoivik N, et al. Electrochemical engineering of hollow nanoarchitectures: pulse/step anodization (Si, Al, Ti) and their applications [J]. Chemical Society Reviews, 2014, 43(5): 1476-1500.

[101] Fabregat-Santiago F, Barea E M, Bisquert J, et al. High carrier density and capacitance in TiO2 nanotube arrays induced by electrochemical doping [J]. Journal of the American Chemical Society, 2008, 130(34): 11312-11316.

[102] Zhou H, Zhang Y. Enhancing the capacitance of TiO_2 nanotube arrays by a facile cathodic reduction process [J]. Journal of Power Sources, 2013, 239: 128-131.

[103] Schuller, J. A. et al. Plasmonics for extreme light concentration and manipulation. Nature Mater. 9, 193–204 (2010).

[104] Atwater, H. A. & Polman, A. Plasmonics for improved photovoltaic devices.Nature Mater. 9, 205–213 (2010).

[105] Linic, S., Aslam, U., Boerigter, C. & Morabito, M. Photochemical transformations on plasmonic metal nanoparticles, Nature Mater. 14, 567–576 (2015).

[106] Langhammer, C., Schwind, M., Kasemo, B. & Zoric, L. Localized surface plasmon resonances in aluminum nanodisks. Nano Lett. 8, 1461–1471 (2008).

[107] Lee, K., Tang, Y. & Ouyang, M. Self-ordered, controlled structure nanoporous membranes using constant current anodization. Nano Lett.8, 4624–4629 (2008).

[108] Prodan, E., Radloff, C., Halas, N. J. & Nordlander, P. A hybridization model for the plasmon response of complex nanostructures. Science 302, 419–422 (2003).

[109] Jeurgens, L. Sloof, W. Tichelaar, F. & Mittemeijer, E. Thermodynamic stabilityof amorphous oxide films on metals: application to aluminum oxide films on aluminum substrates, Phys. Rev. B 62, 4707−4719 (2000).

[110] Xi, J. Q. et al. Optical thin-film materials with low refractive index for broadband elimination of Fresnel reflection. Nature Photon. 1, 176–179 (2007).

[111] Li, K. R., Stockman, M. I. & Bergman, D. J. Self-similar chain of metal nanospheres as an efficient nanolens. Phys. Rev. Lett. 91, 227402 (2003).

[112] B. Jiang, P. Zhang, Y. Zhang, L. Wu, H.X. Li, D.Q. Zhang, G.S. Li, Nanoscale 4 (2012) 455–460.

[113] V. Subramanian, E.E. Wolf, P.V. Kamat, J. Am. Chem. Soc 126 (2004) 4943–4950.

[114] M. Jakob, H. Levanon, P.V. Kamat, Nano Lett. 3 (2003) 353–358.

[115] Z.F. Bian, J. Zhu, F.L. Cao, Y.F. Lu, H.X. Li, Chem. Commun. 378 (2009) 9–3791.

[116] G.S. Li, L. Wu, F. Li, P.P. Xu, D.Q. Zhang, H.X. Li, Nanoscale 5 (2013) 2118–2125.

[117] S.K. Ghosh, T. Pal, Chem. Rev. 107 (2007) 4797–4862.

[118] G.V. Hartland, Chem. Rev. 111 (2011) 3858–3887.

[119] M. Murdoch, G.I.N. Waterhouse, M.A. Nadeem, J.B. Metson, M.A. Keane, R.F. Howe, J. Llorca, H. Idriss, Nat. Chem. 3 (2011) 489–492.

[120] Z.H. Zhang, L.B. Zhang, M.N. Hedhili, H.N. Zhang, P. Wang, Nano Lett. 13 (2013) 14–20.

[121] N. Kruse, S. Chenakin, Appl. Catal. A: Gen. 391 (2011) 367–376.

[122] J.C. Fuggle, N. Martensson, J. Electron. Spectrosc. Relat. Phenom. 21 (1980) 275–281.

[123] M.S. Chandrasekar, M. Shanmugasigamani, Pushpavanam, Mater. Chem. Phys.115 (2009) 603–611.

[124] L.X. Yang, S.L. Luo, F. Su, Y. Xiao, Y.F. Chen, Q.Y. Cai, J. Phys. Chem. C 114 (2010) 7694–7699.

[125] Y.H. Zhang, Y.N. Yang, P. Xiao, X.N. Zhang, L. Lu, L. Li, Mater. Lett. 63 (2009) 2429–2431.

[126] Y.K.Lai, H.F. Zhuang, K.P. Xie, D.G. Gong, Y.X. Tang, L. Sun, C.J. Lin, Z. Chen, New J. Chem. 34 (2010) 1335–1340.

[127] Y. Hou, X.Y. Li, X.J. Zou, X. Quan, G.C. Chen, Environ. Sci. Technol. 43 (2009) 858–863.

[128] G.P. Dai, J.G. Yu, G.H. Liu, Environ. Sci. Technol. 44 (2010) 5098–5103.

[129] Y. Hou, X.Y. Li, Q.D. Zhao, X. Quan, G. Chen, J. Phys. Chem. C 115 (2011) 7339–7346.

[130] M.D. Ye, J.J. Gong, Y.K. Lai, C.J. Lin, Z.Q. Lin, J. Am. Chem. Soc. 134 (2012) 15720–15723.

[131] S.S. Zhang, B.Y. Peng, S.Y. Yang, Y.P. Fang, F. Peng, Int. J. Hydrogen Energ. 38 (2013) 13866–13871.

[132] Y. Hou, X.Y. Li, Q.D. Zhao, G.H. Chen, C.L. Rastor, Environ. Sci. Technol. 46 (2012) 4042–4050.

[133] G.K. Mor, K. Shankar, M. Paulose, O.K. Varghese, C.A. Grimes, Appl. Phys. Lett. 91 (2007) 152111.

[134] A. Corma, P. Serna, H. Garcia, J. Am. Chem. Soc. 129 (2007) 6358–6359.

[135] S. Oros-Ruiz, R. Zanella, R. Lopez, A. Hernandez-Gordillo, R. Gomez, J. Hazard. Mater. 263 (2013) 2–10.

[136] M.S. Chandrasekar, M. Pushpavanam, Electrochim. Acta 53 (2008) 3313–3322.